ORIGINAL RESEARCH

Cardiac CD47 Drives Left Ventricular Heart Failure Through Ca^{2+}-CaMKII-Regulated Induction of HDAC3

Maryam Sharifi-Sanjani, PhD; Ali Hakim Shoushtari, MD; Marisol Quiroz, MS; Jeffrey Baust, BA; Samuel F. Sestito; Mackenzie Mosher, BA; Mark Ross, MS; Charles F. McTiernan, PhD; Claudette M. St. Croix, PhD; Richard A. Bilonick, PhD; Hunter C. Champion, MD, PhD; Jeffrey S. Isenberg, MD, MPH

***Background*—**Left ventricular heart failure (LVHF) remains progressive and fatal and is a formidable health problem because ever-larger numbers of people are diagnosed with this disease. Therapeutics, while relieving symptoms and extending life in some cases, cannot resolve this process and transplant remains the option of last resort for many. Our team has described a widely expressed cell surface receptor (CD47) that is activated by its high-affinity secreted ligand, thrombospondin 1 (TSP1), in acute injury and chronic disease; however, a role for activated CD47 in LVHF has not previously been proposed.

***Methods and Results*—**In experimental LVHF TSP1-CD47 signaling is increased concurrent with up-regulation of cardiac histone deacetylase 3 (HDAC3). Mice mutated to lack CD47 displayed protection from transverse aortic constriction (TAC)-driven LVHF with enhanced cardiac function, decreased cellular hypertrophy and fibrosis, decreased maladaptive autophagy, and decreased expression of HDAC3. In cell culture, treatment of cardiac myocyte CD47 with a TSP1-derived peptide, which binds and activates CD47, increased HDAC3 expression and myocyte hypertrophy in a Ca^{2+}/calmodulin protein kinase II (CaMKII)-dependent manner. Conversely, antibody blocking of CD47 activation, or pharmacologic inhibition of CaMKII, suppressed HDAC3 expression, decreased myocyte hypertrophy, and mitigated established LVHF. Downstream gene suppression of HDAC3 mimicked the protective effects of CD47 blockade and decreased hypertrophy in myocytes and mitigated LVHF in animals.

***Conclusions*—**These data identify a proximate role for the TSP1-CD47 axis in promoting LVHF by CaKMII-mediated up-regulation of HDAC3 and suggest novel therapeutic opportunities. **(*J Am Heart Assoc*. 2014;3:e000670 doi: 10.1161/JAHA.113.000670)**

Key Words: CaKMII • calcium • CD47 • HDAC3 • heart failure • thrombospondin-1

Left ventricular heart failure (LVHF) affects over 5 million people in the United States and includes >650 000 new cases each year, with heart transplantation offered to only ≈2000 patients annually.[1] In less than 30 years, the mortality from LVHF has risen 135%, with the 5-year mortality approaching 50%.[2–4] With the aging of the U.S. population and subsequent increase in incidence, LVHF continues to grow in importance as a public health issue.[5] Despite therapies targeting the neurohormonal activation that accompanies LVHF,[6] the morbidity and mortality associated with cardiac hypertrophy and failure remain high.[3]

We have identified a ligand-receptor interaction, between the secreted matricellular protein, thrombospondin 1 (TSP1), and the widely expressed cell receptor, CD47,[7] that promotes cell injury,[8] in part through inhibition of the nitric oxide (NO)-signaling pathway.[9–12] New data also suggest that TSP1, through CD47, is a direct activator of nicotinamide adenine dinucleotide phosphate (NADPH) oxidase to increase reactive oxygen species (ROS) production.[13] These findings are important because dysregulated NO[14] and pathologic ROS production[15] play a role in promoting heart failure (HF). TSP1 transcript had been reported to be increased[16] and decreased[17] in ventricular biopsies from LVHF patients. However, a role for TSP1-CD47 signaling in LVHF has never been described.

We now find that the TSP1 expression is increased in experimental LVHF. Mice lacking CD47 were protected from transverse aortic constriction (TAC)-driven pressure overload LVHF. Sensitivity to pressure overload-induced LVHF in wild-type (WT) animals correlated with increased expression of

From the Vascular Medicine Institute (M.S.-S., M.Q., J.B., S.F.S., H.C.C., J.S.I.), Division of Pulmonary, Allergy, and Critical Care Medicine (M.S.-S., H.C.C., J.S.I.) and Division of Cardiology, Department of Medicine (C.F.M.), Clinical and Translational Science Institute (A.H.S., H.C.C.), Center for Biologic Imaging (M.M., M.R., C.M.S.C.), Graduate School of Public Health, University of Pittsburgh, Pittsburgh, PA (R.A.B.).

Accompanying Figures S1 through S8 and Video S1 are available at http://jaha.ahajournals.org/content/3/3/e000670/suppl/DC1

Correspondence to: Jeffrey S. Isenberg, MD, MPH, E1258, BST, 200 Lothrop Street, Pittsburgh, PA 15261. E-mail: jsi5@pitt.edu

Received February 4, 2014; accepted April 23, 2014.

calcium/calmodulin-dependent protein kinase II (CaMKII). Downstream analysis of histone deacetylases (HDACs) 1 and 2,[18,19] previously implicated in heart disease, demonstrated HDAC3 suppression concurrent with decreased myocyte hypertrophy and attenuated ventricular fibrosis post-TAC in CD47-null left ventricular (LV) tissue samples. Treating cardiac myocytes with a TSP1-derived peptide (that binds and activates CD47) up-regulated both CaMKII and HDAC3 and stimulated cellular hypertrophy. Conversely, blocking activation of CD47 with a CD47 antagonist antibody (Ab) suppressed HDAC3 expression, decreased cell hypertrophy, and mitigated established LVHF. Finally, in TAC-challenged mice gene suppression of HDAC3 mimicked CD47 blockade and limited myocyte hypertrophy and LVHF. We herein identify activated CD47 as a proximate regulator of HDAC3 signaling to promote LVHF.

Material and Methods

Animals

All experimental protocols were performed according to an approved University of Pittsburgh Institutional Animal Care and Use Committee (IACUC) protocol and National Institutes of Health (NIH; Bethesda, MD) guidelines. Male C57BL6 WT and CD47-null mice (strain B6.129S7-Cd47tm1Fpl/J; The Jackson Laboratory, Bar Harbor, ME) and Sprague-Dawley rats (Charles River Laboratories, Wilmington, MA) were maintained on 12-hour light/dark cycles and had ad libitum access to water and standard rodent chow.

Isolation of Rat Neonatal Cardiac Myocytes

Cardiac myocytes were isolated from ventricular myocardium of 2-day-old Sprague-Dawley rats by enzymatic digestion, as we have described previously.[20]

Human LV Samples

As part of an ongoing investigational protocol approved by the University of Pittsburgh/University of Pittsburgh Medical Center (UPMC; Institutional Review Board [IRB] No.: 0404033), LV samples were obtained from a cohort of nonischemic *end-stage* HF patients (n=4) at the time of HT and control patients (n=5).

TAC Pressure Overload Model and Terminal Hemodynamic Analysis

LVHF was induced in mice by TAC, and after indicated time intervals, terminal hemodynamic analysis was performed by open-chest ventricular catheterization, as we have described previously.[21] After euthanasia, all animals were flushed with normal saline to remove blood from the systemic and pulmonary vasculature before harvesting of LV tissue samples.

Immunohistology

Cryostat sections (5 to 7 μm) were washed three times with PBS, followed by 3 washes of 0.5% BSA in PBS. Sections were blocked with 2% BSA solution for 60 minutes. Slides were incubated with a collagen I Ab at 1:100 dilution in 0.5% BSA solution. Slides were washed with BSA solution and incubated with CY3 goat anti-rabbit secondary Ab in combination with 1:250 dilution of the F-actin dye, rhodamine phalloidin. Nuclei were stained with Hoescht dye for 30 seconds. Images were obtained using an Olympus Fluoview 1000 confocal microscope (Olympus America Inc., Bethlehem, PA) equipped with a ×40 oil (1.3 NA) immersion optic. Rat neonatal cardiac myocytes (RNCMs) were fixed for 20 minutes with 2% paraformaldehyde (PFA), then permeabilized, blocked, and incubated with either primary Ab for HDAC3 (ab16407; Abcam, Cambridge, MA) or pHDAC3 (3815S; Cell Signaling Technology, Danvers, MA), followed by a CY3 goat anti-rabbit secondary Ab (Jackson ImmunoResearch, West Grove, PA) and Alexa 647 phalloidin (Invitrogen, Carlsbad, CA). Nuclei were stained with Hoescht dye. Fluorescent images were captured with an Olympus Fluoview 1000 confocal microscope (software version 2.01; Olympus America Inc.) and analyzed with NIS Elements (version 4.13; Nikon Instruments Inc., Melville, NY).

Assessment of Apoptosis

Apoptosis analysis of LV tissue sections was done employing a terminal deoxynucleotidyl transferase dUTP nick end labeling (TUNEL) assay kit (Roche Molecular Biochemicals, Indianapolis, IN) as per the manufacturer's instructions.

Western Protein Analysis

LV and RNCM homogenates were prepared from tissue or cell samples using ice-cold radioimmunoprecipitation assay (RIPA) lysis buffer, centrifuged, and the supernatant stored at −80°C for future analysis. Protein extracts were separated on 10% Bis-Tris gels or AnyKD precast gels in parallel. Proteins were then transferred to a nitrocellulose membrane, blocked with blocking buffer for 1 hour, and then probed with the respective primary and secondary Abs. Blots were scanned on an Odyssey system imager, and relative band intensities were quantified by densitometry using ImageJ software (NIH), with samples normalized to the corresponding β-actin of lamin B1 values.

Separation of Cell Membrane and Nuclear Fractions

LV and RNCM homogenates were prepared using ice-cold fraction isolation lysis buffer by way of a glass homogenizer and cell scraper, respectively. Homogenates were centrifuged to remove the nucleus. The supernatant was further centrifuged to separate the membrane fraction from the cytosol.

Myocyte Size Analysis

Quantitative image analysis was performed for cardiac myocyte size (hypertrophy) in LV tissue slides and in isolated RNCMs and quantified using image analysis ImageJ software (NIH).

Myocyte Calcium Signaling Analysis

Cells were seeded on 35-mm glass-bottomed dishes and incubated with the calcium indicator, Fluo-4 AM, for 20 minutes, and treated with 0.5 mmol/L of the ryanodine receptor 2 inhibitor, tetracaine hydrochloride, followed by peptide 7N3 (10 μmol/L). Images were acquired employing a closed, thermo-controlled incubator atop the motorized stage of an inverted Nikon TiE fluorescent microscope (Nikon Instruments).

mRNA Analysis

RNA was extracted from human LV samples using a Qiagen RNeasy kit (Qiagen, Germantown, MD). cDNA was generated using the Superscript First-Strand Synthesis System for real-time polymerase chain reaction (RT-PCR). Relative concentrations of TSP1 and CD47 mRNA as well as atrial natriuretic peptide (ANP), B-type natriuretic peptide (BNP), beta myosin heavy chain (β-MHC), and alpha skeletal actin (α-SKA) mRNA were normalized to the housekeeping genes, hypoxanthine phosphoribosyltransferase (HPRT), and β-actin, respectively.

Morpholino Oligonucleotide Gene Suppression

RNMCs were treated for 48 hours with the target or nonspecific oligonucleotide morpholino (20 μmol/L; GeneTools, Philomath, OR). Protein suppression after treatment with the targeting morpholino was confirmed by Western immunoblot of cell lysate.

In Vivo CD47 Blockade

Ten-week-old male C57BL/6 ($CD47^{+/+}$) mice subjected to TAC were treated with a CD47-blocking Ab (clone 301; 0.4 μg/g body weight in 150 μL of sterile normal saline IP weekly; Santa Cruz Biotechnology, Santa Cruz, CA) beginning 1 week postsurgery.

In Vivo HDAC3 Suppression

Ten-week-old male C57BL/6 ($CD47^{+/+}$) mice subjected to TAC were treated with an HDAC3-targeting morpholino (7 mg/kg body weight in 150 μL of sterile normal saline IP) every 4 days beginning 1 week postsurgery.

Statistical Analysis

Statistical analyses were performed using GraphPad Prism software (V6.0; GraphPad Software Inc., La Jolla, CA) and R-3.1.0 (http://cran.cnr.berkeley.edu/). In cases where samples sizes of treatment groups were small (n=3), nonparametric comparison of differences between multiple experimental groups were analyzed by Kruskal-Wallis' test, followed by Dunn's post-hoc test for multiple comparisons. For nonparametric comparison of difference between just two experimental groups, Mann-Whitney's exact test was performed. In other instances, parametric 1-way ANOVA and Tukey's honestly significant different (HSD) post-hoc test for multiple comparisons was performed. $P<0.05$ was used as a criterion for statistical significance.

Detailed Materials and Methods

Reagents

DETA-NO was purchased from Cayman Chemical (Catalog No.: 82120; Cayman Chemical, Ann Arbor, MI). BAY58-2667 was purchased from Biovision (Catalog No.: 2027-1; BioVision Inc., Milpitas, CA).

Animals

All experimental protocols were performed according to an approved University of Pittsburgh IACUC protocol and NIH guidelines. Male C57BL6 WT and CD47-null mice (strain B6.129S7-Cd47tm1Fpl/J; The Jackson Laboratory) and Sprague-Dawley rats (Charles River Laboratories) were maintained on 12-hour light/dark cycles and had ad libitum access to water and standard rodent chow.

Isolation of RNCMs

Cultured cardiac myocytes were isolated from ventricular myocardium of 2-day-old Sprague-Dawley rats by enzymatic digestion, as previously described.[20] In brief, hearts were removed and ventricles were minced in calcium- and bicarbonate-free Hanks' buffer with HEPES. Tissue fragments were

digested by step-wise trypsin dissociation. The dissociated cardiac myocytes were separated from fibroblasts by means of Percoll gradient tube preparation (Sigma-Aldrich, St. Louis, MO). Cells were maintained at 37°C in the presence of 5% CO_2 in a humidified incubator in DMEM+F12 (50/50; cellgro; Corning, Corning, NY), 5% horse serum, gentamicin (Gibco, Grand Island, NY), and insulin-transferin-selenium (Gibco). Bromodeoxyuridine (0.1 mmol/L) was used in the medium for the first 3 days after plating to prevent fibroblast growth. Because the TSP1 promoter has a serum-response element, cells were placed in serum and growth-factor–free medium containing 0.1% BSA for 24 hours before treatments to suppress TSP1 production. In some experiments, cells were treated with autocamtide-2-related inhibitory peptide (AIP; Product No.: 189482; Calbiochem, Millipore Corporation, Billerica, MA), amiloride hydrochloride hydrate (Product No.: A7410; Sigma-Aldrich), or nifedipine (Product No.: N7634; Sigma-Aldrich) 30 minutes before their treatment with 7N3 (FIRVVMYEGKK) or control peptide (VKMKWKYVRF; Peptides International, Louisville, KY).

Human LV Samples

As part of an ongoing investigational protocol approved by the University of Pittsburgh/UPMC (IRB No.: 0404033), LV samples from patients with HF were obtained from a cohort of nonischemic LVHF (n=4) at the time of HT and control (n=5) patients (rapid autopsy or hearts donated for HT that were not used). Samples were immediately snap-frozen in liquid nitrogen and stored at −80°C for later analysis.

Transverse Aortic Arch Pressure Overload Model and Terminal Hemodynamic Analysis

LVHF was induced in mice by TAC, and after indicated time intervals, terminal hemodynamic analysis was performed as previously described.[21] In brief, general anesthesia was induced and maintained with isoflurane inhalation delivered (2.5% in 100% oxygen) by a rodent ventilator with the following settings: 150 to 200 beats per minute and a stroke tidal volume of 250 μL. A thoracotomy was performed and the rib cage retracted to expose the inferior vena cava, the heart, and the great vessels. A 26-gauge needle was used to pierce the LV. The needle was removed and a 1.9-French Scisence (Transonic Systems Inc.; Ithaca, NY) pressure-conductance catheter was then introduced to the LV apex for the measurement of cardiac hemodynamics. Pressure-volume data were acquired using IOX 2.0 software (emka TECHNOLOGIES, Falls Church, VA). After euthanasia, all animals were flushed with normal saline at 4°C to remove red blood and inflammatory cells and platelets from the systemic and pulmonary vasculature before harvesting of LV tissue samples.

Immunohistology

Cryostat sections (5 to 7 μm) were washed 3 times with PBS, followed by 3 washes of 0.5% BSA in PBS. Sections were blocked with 2% BSA solution for 60 minutes. Slides were incubated for 1 hour at room temperature (RT) with the collagen I antibody (polyclonal; Abcam), at 1:100 dilution in 0.5% BSA solution. Slides were washed 3 times with BSA solution and incubated for 1 hour at RT with CY3 goat anti-rabbit secondary Ab (Jackson ImmunoResearch), diluted 1:100 in BSA solution, in combination with 1:250 dilution of F-actin dye rhodamine phalloidin (Invitrogen, Life Technologies, Grand Island, NY). Nuclei were stained with Hoescht dye (bisbenzamide 1 mg/100 mL water) for 30 seconds. After 3 rinses with PBS, sections were coverslipped with Gelvatol mounting media. Images were obtained using an Olympus Fluoview 1000 confocal microscope (Olympus America Inc.) equipped with a ×40 oil immersion optic.

Images were thresholded for collagen and perimyofiber profiles, and the average intensity per pixel within the thresholded region was calculated using NIS Elements (Nikon Instruments). Fluorescence intensity was graded from 0 to 4 with 0 counted as the empty background and 4 as the most intense. RNCM were fixed for 20 minutes with 2% PFA, permeabilized with 0.1% Triton X-100 in PBS, and then washed 3 times with PBS, followed by 3 washes with a solution of 0.5% BSA in PBS. Sections were blocked with 2% goat serum in BSA solution for 30 minutes. Slides were then incubated for 1 hour at RT with either primary Ab for HDAC3 (ab16407; Abcam) or p-HDAC3 (3815S; Cell Signaling Technology) at 1:25 in 0.5% BSA solution. Slides were washed 3 times with BSA solution and incubated for 1 hour at RT with a 1:1000 dilution CY3 goat anti-rabbit secondary Ab (Jackson ImmunoResearch) and 1:250 Alexa 647 phalloidin (Invitrogen). Nuclei were stained with Hoescht dye (bisbenzamide 1 mg/100 mL water) for 30 seconds. After 3 rinses with PBS, sections were coverslipped with Gelvatol mounting media. Fluorescent images were captured with an Olympus Fluoview 1000 confocal microscope (software version 2.01; Olympus America Inc.) and analyzed with NIS Elements (version 4.13; Nikon Instruments).

Western Protein Analysis

LV and RNCM homogenates were prepared from tissue or cell samples using ice-cold RIPA lysis buffer consisting of 0.05 mol/L of Tris-buffered saline (pH 7.4), 1% Triton X-100, 0.25% sodium deoxycholate, 150 mmol/L of sodium chloride, 1 mmol/L of EDTA, 1 mmol/L of phenylmethylsulfonyl, and protease and phosphatase inhibitor cocktails (Roche Molecular Biochemicals) by way of a glass homogenizer. Samples were then centrifuged for 7 minutes at 17 136 rcf and the supernatant stored at −80°C for future analysis. Protein extracts

(25 μg of protein per well) were separated on 10% Bis-Tris gels or AnyKD precast gels (Catalog No.: 456-9031; Bio-Rad, Hercules, CA) in parallel. Proteins were then transferred to a nitocellulose membrane (Bio-Rad), blocked with blocking buffer (LI-COR Biosciences, Lincoln, NE) for 1 hour, and then probed with anti-TSP1 mouse (ab1823, 1:500; Abcam), anti-CD47 mouse (sc-12731, 1:1000; Santa Cruz Biotechnology), anti-p-HDAC3 rabbit, and the following Cell Signaling Technology Abs: anti-HDAC3 mouse (Catalog Nos.: 3815 and 3949, 1:1000); anti-p-CaMKII rabbit and anti-CaMKII rabbit (Catalog Nos.: 3361 and 3357, 1:1000); anti-LC3A rabbit (Catalog No.: 4599) Ab, anti-β-actin (Catalog No.: 4967, 1:2000); or with lamin B1 (Catalog No.: 13435, 1:1000) overnight at 4°C. For RNMCs treated with phenylephrine (PE) or angiotensin-II (Ang II; Sigma-Aldrich) and a CD47 Ab, anti-HDAC3 rabbit (Catalog No.: 2632, 1:1000; Cell Signaling Technology) and anti-CD47 mouse (sc-53050, 1:1000; Santa Cruz Biotechnology) Abs were employed. This was followed by incubation with corresponding secondary fluorescent Abs (LI-COR Biosciences) for 1 hour at RT. Blots were scanned on an Odyssey system imager (LI-COR Biosciences), and relative band intensities were quantified by densitometry using ImageJ software (NIH), with samples normalized to the corresponding β-actin or lamin b1 values.

Apoptosis Analysis

Apoptosis staining was done employing a TUNEL assay kit (Roche Molecular Biochemicals). Cells were incubated with TUNEL reaction mixture at 37°C for 45 minutes, followed by 3 washes with PBS. Cells were incubated with (1:1000 dilution) Alexa 488 streptavidin and (1:250) Alexa 647 phalloidin (Molecular Probes) for 30 minutes at RT. Cells were washed 3 times with PBS and incubated for 30 seconds in Hoescht dye (Sigma-Aldrich), followed by 3 PBS washes and coverslipped with Gelvatol. Image analysis utilized NIS Elements (4.13; Nikon Instruments).

Separation of Cell Membrane and Nuclear Fractions

LV and RNCM homogenates were prepared using ice-cold fraction isolation lysis buffer (buffer A), consisting of 50 mmol/L of Tris-buffered saline, 2 mmol/L of EDTA, and protease inhibitor cocktail and phosphatase inhibitor cocktail (Roche Molecular Biochemicals), by way of a glass homogenizer and scraping off, respectively. This was followed by 5 cycles of freeze/thaw and passage through 20- and 30-gauge needles. Homogenates were centrifuged at 1000 rpm for 10 minutes at 4°C to remove the nucleus. The supernatant was further centrifuged at 50 000 rcf for 1 hour to separate the membrane fraction (pellet) from the cytosol (supernatant). The membrane fraction was resuspended and sonicated with buffer B containing buffer A (300 mmol/L of sodium chloride, 1% Triton X-100, and 0.1% sodium deoxycholate), from which the cytosolic fraction was isolated. Samples were then stored at −80°C for future analysis.

Myocyte Calcium Imaging

Cells were seeded on 35-mm glass-bottomed dishes (MatTek Corporation, Ashland, MA) and incubated with the calcium indicator, Fluo-4 AM (5 μmol/L; Invitrogen, Eugene, OR) for 20 minutes at 37°C. Cells were treated with peptide 7N3 (10 μmol/L)±the ryanodine receptor 2 inhibitor tetracaine hydrochloride (0.5 mmol/L; Catallog No.: T7508; Sigma-Aldrich) for 40 minutes. Cells were washed with Hanks' balanced salt solution, the media replaced, and the dish inserted in a closed, thermo-controlled (37°C) stage-top incubator (Tokai Hit Co., Shizuoka-ken, Japan) atop the motorized stage of an inverted Nikon TiE fluorescent microscope (Nikon Instruments) equipped with a ×60 oil immersion optic (CFI PlanFluor, NA 1.43; Nikon Instruments) and NIS Elements software. Fluo-4 AM was excited using the 470-nm line of a Lumencor diode-pumped light engine (SpectraX; Lumencor Inc., Beaverton, OR) and detected using a ET-GFP filter set (Chroma Technology Corporation, Bellows Falls, VT) and ORCA-Flash4.0 sCMOS camera (Hamamatsu Corporation, Bridgewater, NJ). Data were collected every 3 minutes over a 30-minute period.

Myocyte Size Analysis

Quantitative image analysis was performed for cardiac myocyte size (hypertrophy) of LV tissue slides stained with hematoxylin and eosin (H&E) and isolated RNCM cultures using image analysis ImageJ software (NIH).

mRNA Analysis

RNA was extracted from human and mouse LV samples and RNCMs using the RNeasy kit (Qiagen). cDNA was generated using the Superscript First-Strand Synthesis System for RT-PCR (Invitrogen). RT-PCR reactions for TSP1 and CD47 were carried out using TaqMan Fast Universal PCR Master Mix, according to the manufacturer's protocol (Applied Biosystems, Life Technologies, Grand Island, NY). Thermal cycling conditions were 95.0°C for 0.20 hour, 95.0°C for 0.01 hour, and 60.0°C for 0.20 hour. RT-PCR reactions for β-MHC, α-SKA, β-actin, ANP, and BNP were processed using SYBR Green PCR Master Mix (Applied Biosystems). Data were captured and analyzed on the 7900HT Fast Real-Time PCR System (Applied Biosystems). The relative concentration of TSP1 and CD47 mRNA and ANP, BNP, β-MHC, and α-SKA mRNA were normalized to the housekeeping gene, HPRT, and β-actin respectively. The following primers

sequences from Applied Biosystems were employed: mouse TSP1 (Mm01335418_m1); mouse CD47 (Mm00495005_m1); mouse HPRT1 (Mm00446968_m1); human TSP1 (Hs00962908_m1); human CD47 (Hs00179953_m1); and human HPRT1 (Hs99999909_m1). The following sequences were employed to design primers (Sigma-Aldrich):

Rat
β-MHC-R: 5′-TTCAAAGGCTCCAGGTCTCAGGGC
β-MHC-F: 5′-GCCAACACCAACCTGTCCAAGTTC
α-SKA-R: 5′-ACCACCGGCATCGTGTTGGAT
α-SKA-F: 5′-ATCTCACGTTCAGCTGTGGTCA
BNP-R: 5′-GAACTATGTGCCATCTTGGA
BNP-F: 5′-TCTGCTCCTGCTTTTCCTTA
ANP-R: 5′-GGGCTCCAATCCTGTCAATC
ANP-F: 5′-GCCGGTAGAAGATGAGGTCA
β-actin-R: 5′-TCGGATCCGTGCCACCAGACAGCACTGTGTTG
β-actin-F: 5′-TCGAATTCTGGAGAAGAGCTATGAGCTGCCG
Mouse
β-MHC-R: 5′-TGCAAAGGCTCCAGGTCTGAGGGC
β-MHC-F: 5′-GCCAACACCAACCTGTCCAAGTTC
α-SKA-R: 5′-ATCTCACGTTCAGCTGTGGTCA
α-SKA-F: 5′-ATCTCACGTTCAGCTGTGGTCA
BNP-R: 5′-TCTTGTGCCCAAAGCAGCTT
BNP-F: 5′-ATGGATCTCCTGAAGGTGCT
ANP-R: 5′-AAGAGGGCAGATCTATCGGA
ANP-F: 5′- TTGGCTTCCAGGCCATAATTG
β-actin-R: 5′-CACGGTTGGCCTTAGGGTTCAG
β-actin-F: 5′-GCTGTATTCCCCTCCATCGTG

In Vivo CD47 Suppression

Ten-week-old male C57BL/6 ($CD47^{+/+}$) mice subjected to TAC were injected with a CD47 antagonist Ab (clone 301; 0.4 μg/g body weight in 150 μL of sterile normal saline IP weekly; Santa Cruz Biotechnology) beginning 1 week postsurgery.

In Vivo HDAC3 Suppression

A HDAC3 specific morpholino oligonucleotide with the following base-pair sequence ACCAGGCCCCGAGCCTCAGCT from 5′ to 3′ was prepared by GeneTools (Philomath, OR). Ten-week-old male C57BL/6 ($CD47^{+/+}$) mice subjected to TAC were treated with the morpholino (10 mg/kg body weight in 100 μL of sterile normal saline IP) twice-weekly beginning 1 week postsurgery.

Statistical Analysis

Statistical analyses were performed using GraphPad Prism software (V6.0; GraphPad Software Inc.) and R-3.1.0 (http://cran.cnr.berkeley.edu/). In cases where samples sizes of treatment groups were small (n=3), nonparametric comparison of differences between multiple experimental groups were analyzed by Kruskal-Wallis' test followed by Dunn's post-hoc test for multiple comparisons. For nonparametric comparison of difference between just two experimental groups, Mann-Whitney's exact test was performed. In other instances, parametric 1-way ANOVA and Tukey's HSD post-hoc test for multiple comparisons was performed. $P<0.05$ was used as a criterion for statistical significance.

Results

TSP1-CD47 Signaling Is Increased in LVHF

Expression of matricellular proteins in general, and TSP1 specifically, in HF is little studied and CD47 has not previously been assessed in the setting of LVHF. In an experimental model of TAC-induced pressure overload LVHF, TSP1 protein, but not mRNA (Figure 1A and1C), was increased at 4 weeks after TAC in WT C57BL/6 mice, whereas CD47 protein and mRNA levels remained stable (Figure 1B and 1D). Interestingly, in CD47-null mice, which lack the ability to produce functional protein, but not transcript, LV mRNA transcript levels of CD47 were decreased both pre- and post-TAC, compared to WT (Figure 1D).

CD47 Promotes LVHF

To assess the role of CD47 in LVHF WT ($CD47^{+/+}$) and CD47-null ($CD47^{-/-}$), C57BL/6 age-matched male mice were challenged

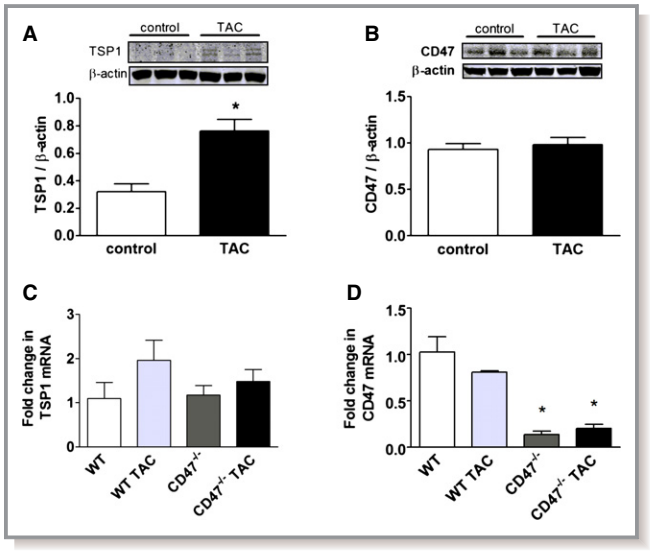

Figure 1. TSP1-CD47 signaling is up-regulated in LVHF. Western immunoblot analysis of protein expression (A and B) and mRNA transcript (C and D) levels of TSP1 and CD47 left ventricle samples from wild-type (WT) and CD47 ($^{-/-}$) null mice pre- and 4 weeks post-TAC. Data are presented as the mean (±SEM; n=3 to 7 animals/group). *=statistically significant difference ($P<0.05$), compared to control and WT and WT TAC. LVHF indicates left ventricular heart failure; TAC, transverse aortic constriction; TSP1, thrombospondin 1.

with 4 weeks of TAC. Histologic assessment demonstrated cardiac myocyte hypertrophy post-TAC in WT LV tissue sections, compared to CD47-null samples (Figure 2A). WT LV tissue sections also displayed increased extracellular collagen matrix deposition (Figure 2B) and corresponded to higher LV weights in WT versus CD47-null hearts post-TAC (Figure 2C). Because body weight can directly affect organ size, we normalized LV weight to body weight and found that WT LV weights were still greater than CD47-null LV weights post-TAC (Figure 2C). TAC-challenged CD47-null mice had enhanced cardiac function, including a trend toward greater cardiac output, significantly better systolic function (quantified by the contractility index), and less diastolic dysfunction (determined by the change in pressure over the change in time [dP/dt_{min}]), compared to TAC-challenged WT mice (Figure 2D). TAC-challenged CD47-null mice also displayed pressure volume loop profiles that more closely resembled non-TAC animals (Figure 2E). Interestingly, LV expression of TSP1 protein (Figure 2F) and mRNA (Figure 1C) were not increased post-TAC in CD47-null mice or significantly detected, compared to WT for that matter (Figure 1A). HF is associated with myocyte apoptosis.[22] In keeping with protection from TAC-mediated LVHF, LV samples from CD47-null mice displayed less evidence of cellular apoptosis, as quantified by fewer TUNEL staining positive cells, compared to LV samples from WT post-TAC animals (Figure 2G).

CD47 Increases HDAC3 Expression Under Basal and LVHF Conditions

HDACs have a role in controlling cardiac responses to stress,[23] and class I HDACs are being investigated as therapeutic targets in HF.[24,25] HDAC3, however, has not previously been linked to LVHF. New data demonstrate induction of HDAC3 in an experimental model of LVHF (Figure 3A). CD47-null animals displayed no elevation in HDAC3 expression post-TAC (Figure 3A). Interestingly, in control CD47-null mice, LV HDAC3 expression was below levels in control WT animals. Phosphorylated HDAC3 (p-HDAC3) was unchanged in all groups (Figure 3A). CD47 regulation of HDAC3 appears to be specific because HDAC1, -2, and -4 were not significantly altered in expression post-TAC in CD47-null LV samples, compared to WT (Figure S1). In patient samples, both phosphorylated and total HDAC3 were decreased in *end-stage* LVHF, compared to controls (Figure 3B).

Activation of CD47 Stimulates Increased HDAC3 Expression and Cardiac Myocyte Hypertrophy

TSP1 has several functional domains that can engage a number of cell surface receptors, including CD47.[26] To confirm the proximate location of CD47 in this signaling cascade, we treated cardiac myocytes with a peptide derived from the C-terminal of TSP1 (peptide 7N3, FIRVVMYEGKK) that we and others have shown activates CD47.[27,28] Treatment of cardiac myocytes with peptide 7N3 (10 μmol/L) increased HDAC3 expression within 1 hour (Figure 3C). To test whether CD47 also regulated HDAC3 induction by known agonists of cardiac hypertrophy and LVHF, cardiac myocytes were challenged with Ang II or PE (10 μmol/L for 48 hours) ± a CD47 antagonist Ab (clone OX101, 1 μg/mL) that, as we published, blocks activation of CD47.[29] HADC3 protein expression was increased in cardiac myocytes after Ang II treatment, whereas treatment with a CD47 antagonist Ab suppressed this, though results did not reach significance on nonparametric analysis (Figure 3D). Additionally, treatment with CD47 antagonist Ab significantly lowered HDAC3 protein levels in PE-stimulated myocytes (Figure S2). To confirm the role of HDAC3 in promoting CD47-mediated cell hypertrophy, we treated cardiac myocytes with a specific HDAC3 gene-suppressing oligonucleotide morpholino or a control nontargeting morpholino (CTRL). Morpholino treatment resulted in a concentration-dependent decrease in HDAC3 protein expression, as confirmed by Western immunoblot (Figure S3A). Treatment with the CD47-activating peptide, 7N3 (10 μmol/L) stimulated myocyte hypertrophy, and this effect was mitigated in myocytes pretreated with the HDAC3 gene-suppressing morpholino (Figure 3E).

CD47 Regulation of HADC3 Is Likely Not Through Inhibition of NO

HF is ameliorated through enhanced NO/cyclic guanylyl cyclase (sGC) signaling.[30] Conversely, activated CD47 is known to inhibit NO-sGC signaling.[10,31] This suggested that perhaps CD47-mediated up-regulation of HDAC3, and promotion of LVHF, was through inhibition of NO-sGC signaling. To test this, we treated cardiac myocytes, which lack a constitutive NO synthase, with the primary NO donor compound, 2,2′-(hydroxynitrosohydrazono)bis-ethanimine (DETA-NO; 10 μmol/L), with or without the CD47-activating peptide, 7N3 (10 μmol/L), and assessed phosphorylated (p-) and total HDAC3 protein expression. After a 3-hour treatment with exogenous NO, p-HDAC3 and total HDAC3 protein levels were decreased (Figure 3F), though results did not reach significance on nonparametric analysis. Pretreatment with the CD47-activating peptide, 7N3 (10 μmol/L), had no effect on NO-treated cells, suggesting that activated CD47 regulates HDAC3 signaling independently of its known inhibitory effects on NO-sGC signaling. Treatment of cardiac myocytes with the non-NO-dependent sGC activator, BAY58-2667[32] (1 μmol/L), for 3 hours also decreased HADC3 protein expression, though results did not reach significance on nonparametric analysis, suggesting that this effect is mediated by the sGC second messenger, cyclic guanosine monophosphate (Figure S3B).

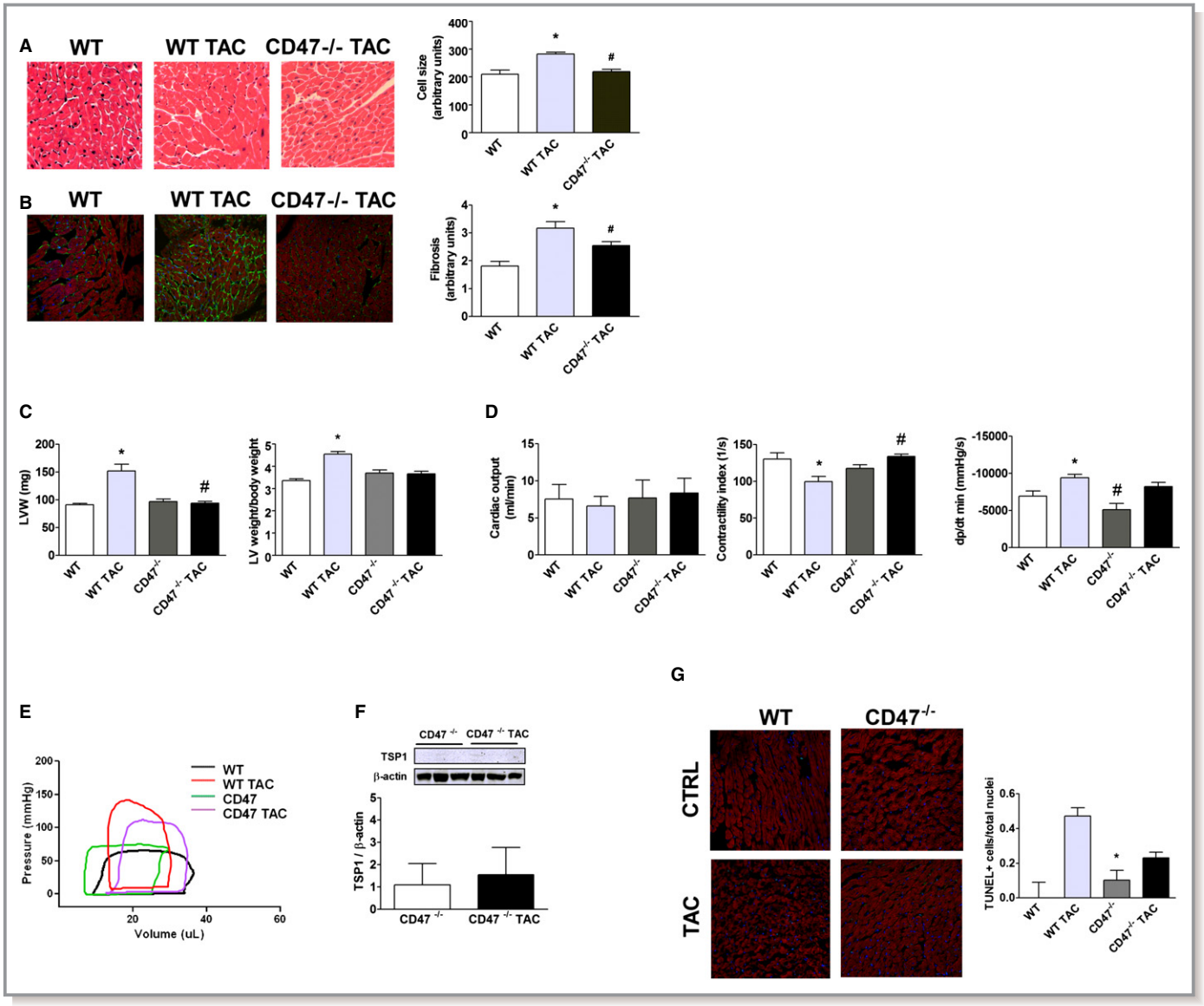

Figure 2. CD47 promotes LVHF. A, H&E staining of murine left ventricle tissue sections from wild-type (WT) and CD47 ($^{-/-}$) null mice 4 weeks post-TAC and controls. Cell-size quantification is presented as the mean (±SEM) of analysis of 4 to 5 slides per animal sample, 10 random hpf per slide, 4 to 5 animals per treatment group. *=statistically significant difference (P<0.05), compared to WT; #=statistically significant difference (P<0.05), compared to WT TAC. Representative images are presented (original magnification, ×40). B, Immunofluorescence staining of murine left ventricle tissue sections 4 weeks post-TAC or control. DAPI, collagen I, and phalloidin colored blue, green, and red, respectively. Fibrosis is calculated as intensity of fluorescence and is presented as the mean (±SEM) of analysis of 3 to 5 slides per animal sample, 10 random hpf per slide, 4 to 7 animals per treatment group. *=statistically significant difference (P<0.05), compared to WT; #=statistically significant difference (P<0.05), compared to WT TAC. Representative images are presented (original magnification, ×40). C, Left ventricle weights (LVW) and LV to body weight from animals 4 weeks post-TAC or controls. Data are presented as the mean (±SEM) of n=7 to 12 animals per group. *=statistically significant difference (P<0.05), compared to WT; #=statistically significant difference (P<0.05), compared to WT TAC. D, Assessment by open-chest pressure volume loop analysis of cardiac output, contractility, and ventricular stiffness (dp/dt min) of animals 4 weeks post-TAC or control. Data are presented as the mean (±SEM) of n=7 to 12 animals/group. *=statistically significant difference (P<0.05), compared to WT; #=statistically significant difference (P<0.05), compared to WT TAC. E, Representative pressure volume tracings are shown from age-matched male WT and CD47-null mice at baseline and post-TAC. F, Western immunoblot analysis of TSP1 expression in left ventricular samples from CD47 null mice 4 weeks post-TAC or control. Data are presented as the mean (±SEM; n=3 to 6 animals per group). G, TUNEL staining of murine left ventricle tissue sections from control WT and CD47-null animals (CTRL) and 4 weeks post-TAC. Data are presented as the mean (±SEM) of the ratio of TUNEL positive cells over total nuclei from analysis of 4 to 5 slides per animal sample, 10 random hpf per slide, 3 to 4 animals per treatment group. *=statistically significant difference (P<0.05), compared to WT TAC. DAPI indicates 4', 6-diamidino-2-phenylindole; H&E, hematoxylin and eosin; LVHF, left ventricular heart failure; TAC, transverse aortic constriction; TSP1, thrombospondin 1; TUNEL, terminal deoxynucleotidyl transferase dUTP nick end labeling.

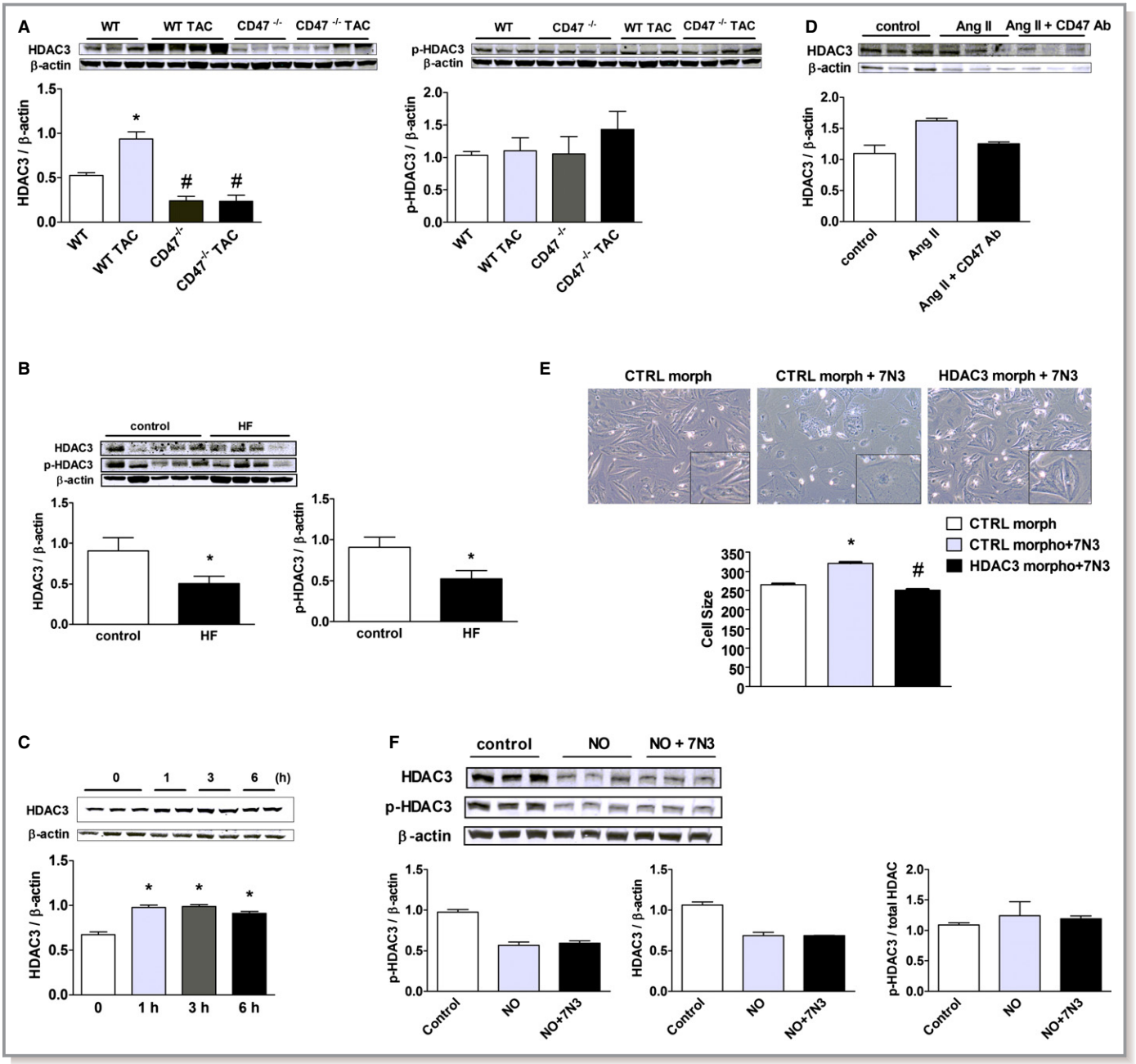

Figure 3. CD47 up-regulates HDAC 3 in LVHF. A, Western immunoblot analysis of HDAC3 and phosphorylated (p-)HDAC3 expression in LV samples from wild-type (WT) and CD47 ($^{-/-}$) null animals 4 weeks post-TAC or control. Densitometry is presented as the mean (±SEM) of n=6 to 9 animals per group. *=statistically significant difference (P<0.05), compared to WT; #=statistically significant difference (P<0.05), compared to WT TAC. B, Western immunoblot analysis of HDAC3 and phosphorylated HDAC3 (p-HDAC3) expression in left ventricular samples from end-stage nonischemic LVHF (n=4) and control (n=5) patients. Densitometry is presented as the mean (±SEM). *=statistically significant difference (P<0.05), compared to control. C, Rat neonatal cardiac myocytes (RNCMs) were treated with the TSP1-based CD47-activating peptide, 7N3 (10 μmol/L), for the indicated time points (h=hours) or (D) angiotensin II (Ang II; 10 μmol/L for 48 hours)±a CD47 antagonist antibody (Ab; clone OX101, 1 μg/mL) and Western immunoblot analysis of HDAC3 protein expression performed on cell lysates. Representative blots are shown. Densitometry is presented as the mean (±SEM) of n=3 experiments. *=statistically significant difference (P<0.05), compared to untreated. E, RNCMs were treated with a HDAC3 or control (CTRL) morpholino oligonucleotide (20 mmol/L)±peptide 7N3 (10 μmol/L) for 48 hours and cell size assessed. Representative images are presented (original magnification, ×40). Data are presented as the mean (±SEM) of 4 separate experiments. *=statistically significant difference (P<0.05), compared to CTRL morpholino; #=statistically significant difference (P<0.05), compared to CTRL morpholino+7N3. F, RNCMs were treated with the CD47-activating peptide, 7N3 (10 μmol/L)±DETA-NO (10 μmol/L), for 3 hours, and Western immunoblot analysis of total and phosphorylated HDAC3 (p-HDAC3) protein expression was performed on cell lysates. Representative blots are shown. Densitometry is presented as the mean (±SEM) of n=3 experiments. HDAC indicates histone deacetylases; LVHF, left ventricular heart failure; TAC, transverse aortic constriction; TSP1, thrombospondin 1.

Activated CD47 Promotes Decreased Cytosolic and Increased Nuclear HDAC3 Expression In Vivo and In Vitro

HDACs regulate cell responses through trafficking between the cytoplasm and the nucleus.[33] Western blot analysis of LV samples from the indicated treatment groups showed, both at baseline and post-TAC, that total HDAC3 was decreased in the nuclear fraction of CD47-null LV samples, compared to WT (Figure 4A). HDAC3 was also decreased in CD47-null LV tissue cytosolic fractions post-TAC (Figure 4B). Western immunoblots of cultured WT ($CD47^{+/+}$) myocytes treated with the CD47-activating peptide, 7N3 (10 μmol/L, 3 hours), displayed increased nuclear-to-cytosol HDAC3 (Figure 4C) and phosphorylated HDAC3 (p-HDAC3) (Figure 4D). To further confirm these data, RNMCs were treated with peptide 7N3 (10 μmol/L) for 3 and 24 hours, respectively, and immunohistochemistry (IHC) analysis performed. Consistent with results obtained by Western immunoblot analysis, on IHC, 7N3-treated RNMCs demonstrated increased nuclear staining for total HDAC3, compared to untreated cells at 3 and 24 hours, and for p-HDAC3, compared to untreated cells at 3 hous (Figure 4E). Finally, we challenged WT mice with TAC for 1 week and then intervened to interrupt CD47 signaling by treating animals with a CD47 antagonist Ab (clone 301, 0.4 μg/g body weight IP weekly for 3 weeks).[34] Importantly, we found increased nuclear HDAC3 expression in LV tissue from WT TAC mice, whereas HDAC3 was decreased in samples from animals treated with the CD47 Ab post-TAC (Figure 4F).

Gene Suppression of HDAC3 Mitigates LVHF

To determine whether HDAC3 is sufficient to induce LVHF, we treated WT mice with a specific HDAC3 gene-suppressing morpholino oligonucleotide. Mice treated with the HDAC3-targeting morpholino (7 mg/kg body weight in 150 μL of sterile normal saline IP every 4 days beginning 1 week after TAC and continuing for 3 weeks) were resistant to TAC-mediated LV myocyte hypertrophy and fibrosis (Figure 5A and 5B). Similarly, HDAC3 morpholino-treated mice displayed increased cardiac output (Figure 5C), decreased LV weights (Figure 5D), and less change in their pressure volume loop profile post-TAC, compared to untreated TAC animals (Figure 5E). Consistent with the improvement in cardiac function, Western immunoblot analysis of protein expression in LV tissue samples from HDAC3 morpholino-treated mice demonstrated decreased TSP1, CD47, and HDAC3 expression post-TAC (Figure 5F through 5H). Additionally, myocytes treated with a CD47-blocking Ab (clone OX010, 1 μg/mL) were insensitive to 7N3-stimulated increases in HDAC3 expression (Figure 5I), locating CD47 upstream in this process. Post-TAC, TUNEL-positive staining cells were increased in LV tissue samples from WT mice, compared to samples from WT animals treated with the HDAC3 morpholino (Figure 5J).

Activated CD47 Stimulates Up-regulation of CaMKII to Increase HDAC3 Expression

CaMKII is dysregulated in HF,[35] stimulates downstream targets, including HDAC,[36] and promotes myocyte hypertrophy.[37] In human end-stage LVHF samples, total and phosphorylated CaKMII (p-CAKMII) were decreased, though the ratio of phosphorylated to total CaKMII was elevated, compared to controls (Figure 6A). In WT mice LV tissue samples, CaMKII is induced post-TAC, whereas in samples from CD47-null mice, CaMKII expression was suppressed, though results in null samples did not reach significance (Figure 6B). Interestingly, in LV tissue samples, TAC-mediated increases in phosphorylated and total CaMKII were suppressed in WT mice treated with an HADC3 morpholino (Figure S5A). To further interrogate the signaling behind these results, we treated cultured $CD47^{+/+}$ cardiac myocytes with the CD47-activating peptide (peptide 7N3, 10 μmol/L). In time-course experiments, peptide-treated cells demonstrated increased expression of phosphorylated and total CaMKII expression (Figure 6C). The ratio of phosphorylated to total CaMKII protein was also increased in cells treated with the CD47-activating peptide. Conversely, treating cardiac myocytes with a CD47 antagonist Ab blocked the 7N3-stimulated increase in p-CaMKII (Figure 6D). Finally, treatment of myocytes with AIP (10 nmol/L, 30 minutes), a specific inhibitor of CaKMII, blocked the 7N3-stimulated increase in HDAC3 (Figure 6E), placing CaKMII downstream of CD47, but upstream of HDAC3, in this signaling cascade. CaMKII, through HDACs, is known to regulate several proteins, including ANP, BNP, β-MHC, and α-SKA, to promote myocyte hypertrophy.[38,39] To investigate this, we assessed mRNA levels of several of these target genes, including β-MHC, ANP, and α-SKA, in LV samples from mice (Figure S4A through S4C). Interestingly, mRNA transcript levels of β-MHC, ANP, and α-SKA were decreased in CD47-null LV samples and Ab- and morpholino-treated WT LV samples, compared to untreated WT post-TAC LV samples, though results did not reach significance on nonparametric analysis. BNP mRNA levels were unchanged between treatment groups (Figure S4D). RNMCs treated with peptide 7N3 (10 μmol/L) for 3 hours showed a trend toward increased levels of β-MHC and BNP mRNA, compared to untreated cells, though differences did not reach statistical significance (Figure S4E and S4F).

Activated CD47 Modulates Cardiac Myocyte Ca^{2+} to Control CaMKII

CaKMII is a Ca^{2+}-dependent enzyme,[40] and we reported on a role for TSP1 in regulating Ca^{2+} flux in vascular endothelial

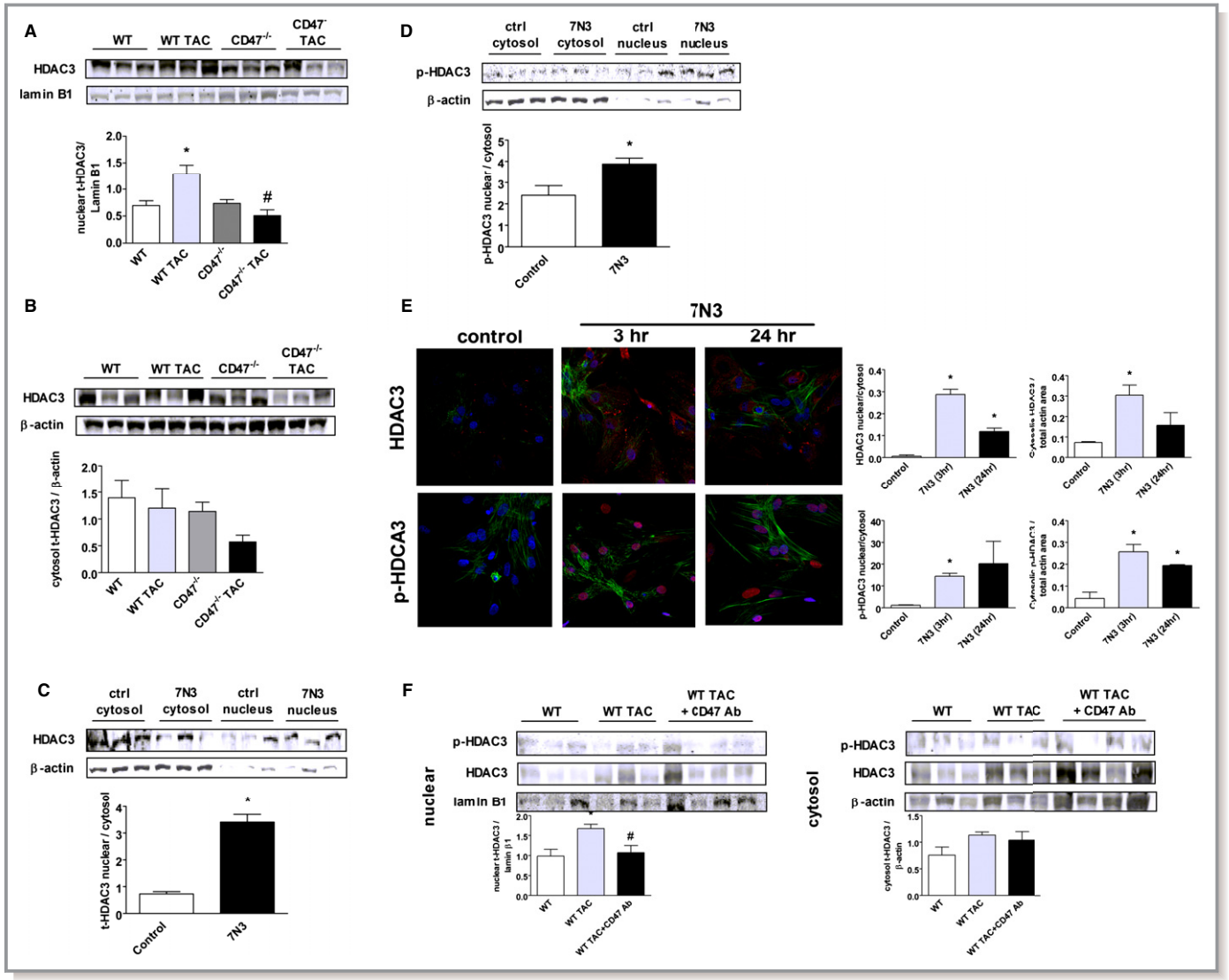

Figure 4. Activated CD47 promotes decreased cytosolic and increased nuclear HDAC3 expression. Western immunoblots of nuclear (A) and cytosolic (B) HDAC3 expression in LV tissue samples from wild-type (WT) and CD47 ($^{-/-}$) null animals 4 weeks post-TAC or control. Densitometry is presented as the mean (±SEM) of n=6 to 9 animals per group. *=statistically significant difference (P<0.05), compared to WT; #=statistically significant difference (P<0.05), compared to WT TAC. Rat neonatal cardiac myocytes (RNCMs) were treated with peptide 7N3 (10 μmol/L) for 3 hours, and Western immunoblot analysis of cytosolic and nuclear total HDAC3 (t-HDAC3) (C) and cytosolic and nuclear phosphorylated HDAC3 (p-HDAC3) (D) protein expression was performed. Densitometry is presented as the mean (±SEM) of n=6 to 9 separate experiments. *=statistically significant difference (P<0.05), compared to control. E, Immunofluorescence staining of RNCMs treated with peptide 7N3 (10 μmol/L) for 3 and 24 hours, respectively. DAPI, total HDAC3, and p-HDAC3, and actin are colored blue, red, and green, respectively. Stained area of fluorescence is presented as the mean (±SEM) of analysis of multiple (>3) regions of interest (ROIs) per culture dish with n=a minimum of 4 cells per ROI. Fluorescent images were captured with an Olympus Fluoview 1000 confocal microscope (software version 2.01; Olympus America Inc., Bethlehem, PA) and analyzed with NIS Elements (version 4.13; Nikon Instruments, Inc., Melville, NY) and calculated as total red (p- or t-HDAC3) area in nuclei/total red (p- or t-HDAC3) area in cytosol. *=statistically significant difference (P<0.05), compared to control. F, Western immunoblots of nuclear and cytosolic HDAC3 expression in LV tissue samples from WT mice±a CD47 antagonist antibody (Ab) (clone 301, 0.4 μg/g body weight IP weekly for 3 weeks). Animals underwent TAC for 1 week before beginning Ab treatment. Densitometry is presented as the mean (±SEM) of n=6 to 9 animals per group. *=statistically significant difference (P<0.05), compared to WT; #=statistically significant difference (P<0.05), compared to WT TAC. HDAC indicates histone deacetylases; LV, left ventricle; TAC, transverse aortic constriction.

cells.[12] However, the role of CD47 in controlling cardiac myocyte Ca^{2+} is unknown. To test this, we loaded cardiac myocytes with the calcium-sensitive dye, Fluro-4, treated them with peptide 7N3 (10 μmol/L), and assessed changes in fluorescent intensity. Treatment with 7N3 resulted in a rapid increase in cellular cytosolic calcium (Video S1) that was mitigated by the ryanodine receptor 2 (RyR2)-blocker, tetracaine (Figure 6F). These data suggest that activation of CD47

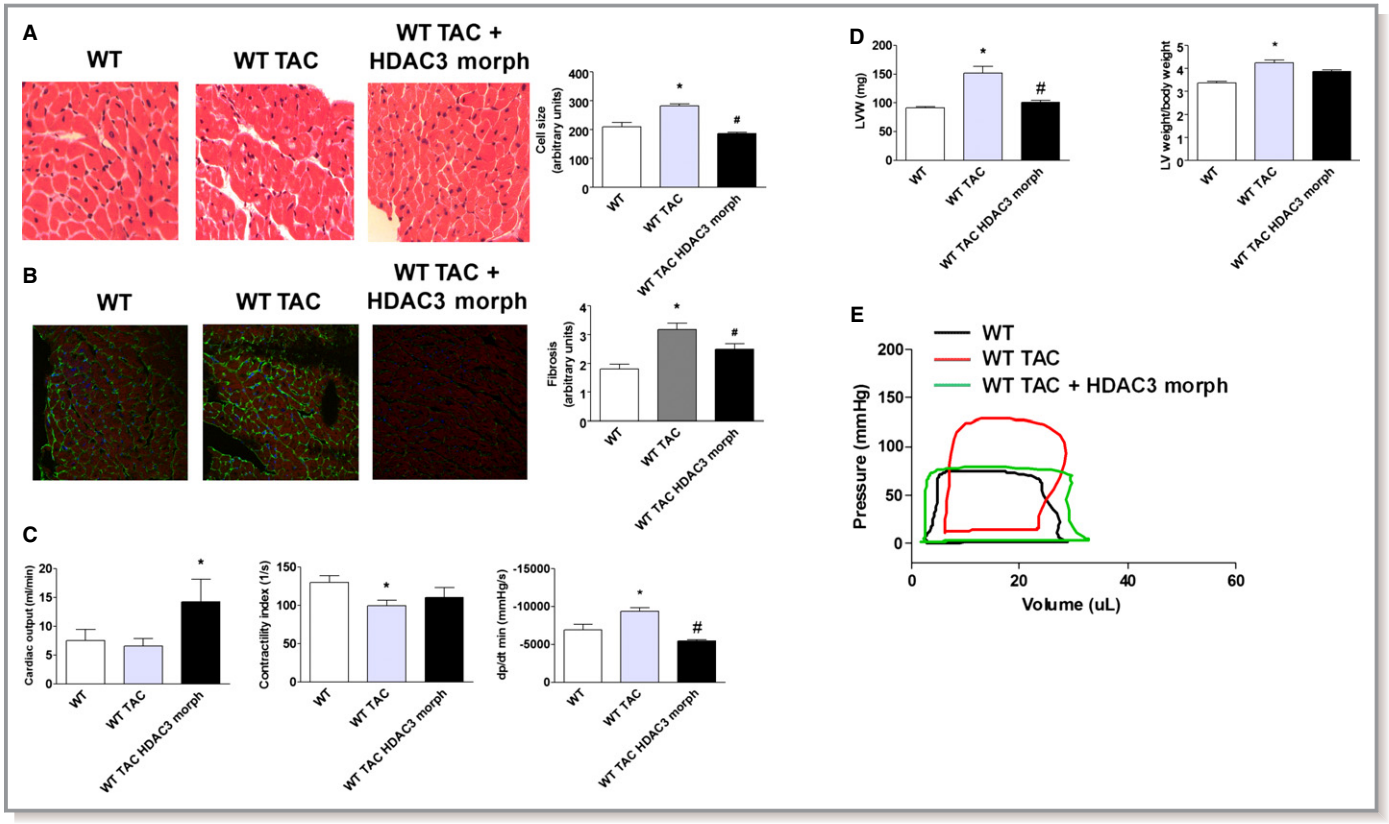

Figure 5. Gene suppression of HDAC3 mitigates LVHF. A, H&E staining of murine left ventricle tissue sections 4 weeks post-TAC or post-TAC followed 1 week later with HDAC3 morpholino treatment. Cell-size quantification is presented as the mean (±SEM) of analysis of 4 to 5 slides per animal sample, 10 random hpf per slide, 3 to 4 animals per treatment group. *=statistically significant difference ($P<0.05$), compared to wild-type (WT); #=statistically significant difference ($P<0.05$), compared to WT TAC. Representative images are presented (original magnification, ×40). B, Immunofluorescence staining of murine left ventricle tissue sections 4 weeks post-TAC or post-TAC followed 1 week later with HDAC3 morpholino treatment. DAPI, collagen I, and phalloidin are colored blue, green, and red, respectively. Fibrosis is calculated as intensity of fluorescence and is presented as the mean (±SEM) of analysis of 4 to 5 slides per animal sample, 10 random hpf per slide, 4 to 8 animals per treatment group. *=statistically significant difference ($P<0.05$), compared to WT; #=statistically significant difference ($P<0.05$), compared to WT TAC. Representative images are presented (original magnification, ×40). C, Assessment by open-chest pressure volume loop analysis of cardiac output, contractility, and ventricular stiffness (dp/dt min) of animals from the indicated groups. Data are presented as the mean (±SEM) of n=4 to 12 animals/group. *=statistically significant difference ($P<0.05$), compared to WT and WT TAC, respectively; #=statistically significant difference ($P<0.05$), compared to WT TAC. D, Left ventricle weights alone and normalized to body weight from animals in treatment groups as in A. Data are presented as the mean (±SEM) of n=4 to 12 animals/group. *=statistically significant difference ($P<0.05$), compared to WT; #=statistically significant difference ($P<0.05$), compared to WT TAC. E, Representative pressure volume tracings are shown from WT, WT TAC, and WT TAC+HDAC3 morpholino-treated mice. Western immunoblot analysis of HDAC3 (F), TSP1 (G), and CD47 (H) protein expression in LV samples from animals in the indicated groups. Densitometry is presented as the mean (±SEM) of n=4 to 9 animals/group. *=statistically significant difference ($P<0.05$), compared to control; #=statistically significant difference ($P<0.05$), compared to WT TAC. I, Rat neonatal cardiac myocytes were treated with a CD47 antibody (Ab; clone OX101, 1 mg/mL)±peptide 7N3 (10 μmol/L) for 48 hours, and expression of total HDAC3 and phosphorylated HDAC3 (p-HDAC3) by Western immunoblot was determined. Densitometry is presented as the mean (±SEM) of 3 separate experiments. *=statistically significant difference ($P<0.05$), compared to 7N3+CD47 Ab treated. J, TUNEL staining of murine LV tissue sections from WT and 4 weeks post-TAC animals with and without HDAC3 morpholino treatment. Data are presented as the mean (±SEM) of the ratio of TUNEL-positive cells over total nuclei from analysis of 4 to 5 slides per animal sample, 10 random hpf per slide, 3 to 4 animals per treatment group. *=statistically significant difference ($P<0.05$), compared to WT TAC. DAPI indicates 4',6-diamidino-2-phenylindole; HDAC, histone deacetylase; H&E, hematoxylin and eosin; LVHF, left ventricular heart failure; TAC, transverse aortic constriction; TSP1, thrombospondin-1; TUNEL, terminal deoxynucleotidyl transferase dUTP nick end labeling.

stimulates acute elevation in myocyte cytoplasmic [Ca^{2+}], through stimulating ryanodine receptors to release Ca^{2+} from the sarcoplasmic reticular (SR) membrane. This finding is interesting because RyR2 receptor dysfunction contributes to LVHF,[41] and they are themselves targets for regulation by CaMKII.[42] Restoration of cytosolic [Ca^{2+}] to baseline is effected by the sarcoplasmic/endoplasmic reticulum ATPase (SERCA) pump.[43] LV samples from CD47-null and WT mice showed comparable SERCA protein expression (data not shown). In contrast, phosphorylated phospholamban (p-PLB) was significantly decreased post-TAC in LV samples from CD47-null mice, compared to samples from WT mice

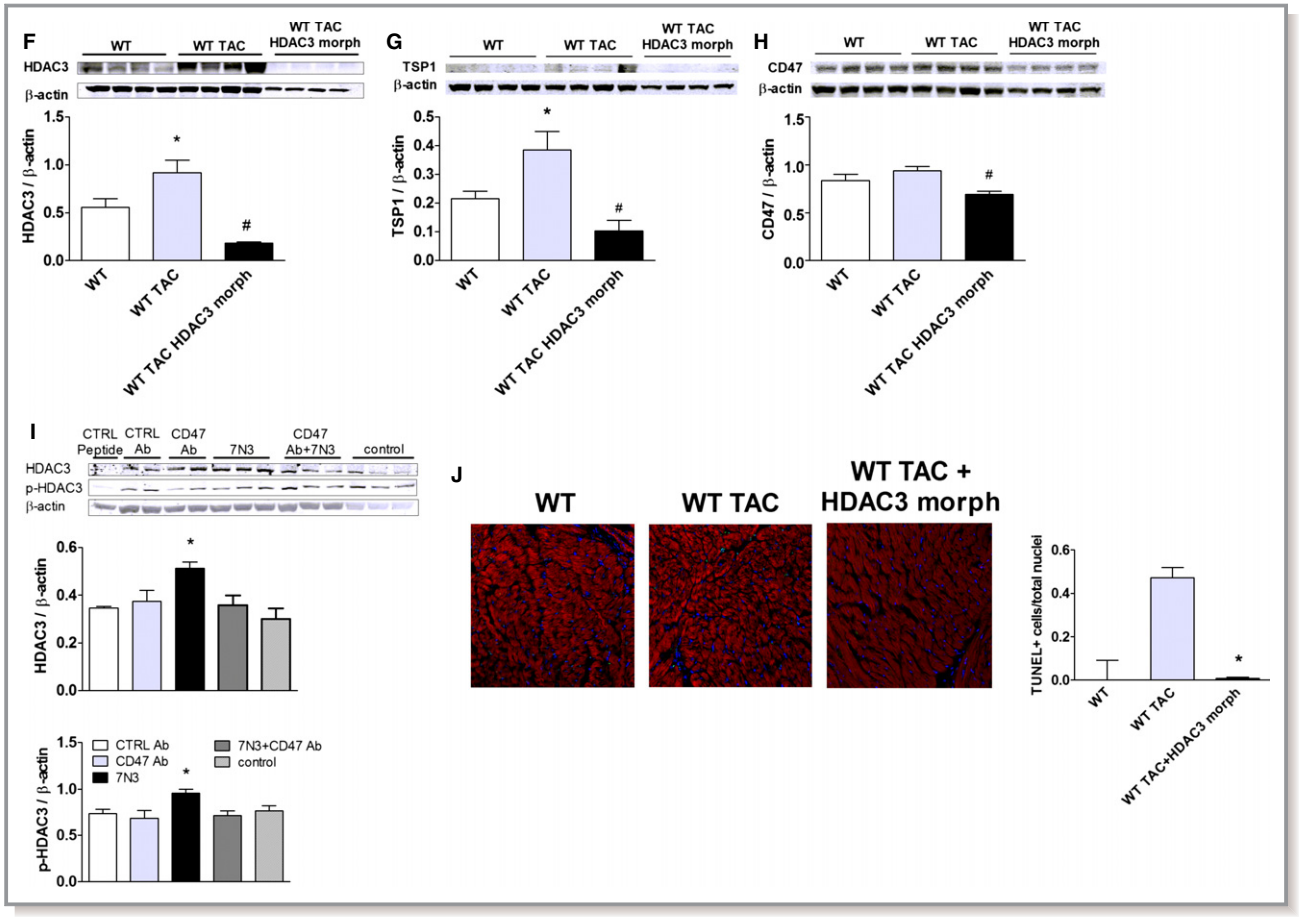

Figure 5. (Continued).

(Figure 6G), whereas total phospholamban was unchanged. This finding is important because decreased p-PLB levels are reported to protect mice from HF,[44] whereas suppressing PLB improved calcium handling and contraction of human myocytes.[45] Finally, cardiac myocytes treated with the Na^+/Ca^{2+} exchanger blocker, amiloride (5 μmol/L, 30 minutes), were insensitive to 7N3-mediated stimulation of CaKMII expression (Figure S5B). Likewise, amiloride treatment blocked 7N3-stimulated increases in HDAC3 and p-HDAC3 expression in cardiac myocytes (Figure S5C). Additionally, treatment with the L-type calcium channel blocker, nifedipine (10 μmol/L, 30 minutes), inhibited 7N3-mediated effects on total and p-CaKMII (Figure S5D). Together, these data suggest that activated CD47 promotes inward movement of Ca^{2+} through membrane myocyte L-type calcium channels to stimulate RyR2 receptor SR-mediated increases in cytosolic [Ca^{2+}].

Activated CD47 Promotes Accumulation of Autophagy Markers in LVHF

Cardiac myocytes respond to stress through several compensatory mechanisms, including autophagy,[46] dysregulated autophagy promotes LVHF,[47] and Ca^{2+} modulates autophagy.[48] We now report on decreased expression of the autophagy marker, microtubule-associated protein 1 light chain 3 form A (LC3), in LV samples from *end-stage* human hearts, compared to controls (Figure 7A). In experimental HF, LC3 is increased,[49,50] whereas suppression of autophagy protects myocytes from injury.[51] Consistent with this, we found increased LV expression of LC3 in WT mice post-TAC (Figure 7B) and LC3 expression increased for up to 4 weeks post-TAC (Figure 7D). In contrast, in CD47-null animals, LV expression of LC3 was decreased post-TAC, but did not reach statistical significance on nonparametric analysis (Figure 7C). Likewise, systemic treatment of WT ($CD47^{+/+}$) mice with a HDCA3 morpholino (7 mg/kg body weight in 150 μL of sterile normal saline IP every 4 days for 4 weeks) (Figure 7D) or a CD47-blocking Ab (clone 301, 0.4 μg/kg body weight IP weekly for 4 weeks) (Figure 7E) resulted in decreased LV expression of LC3, autophagy related gene (ATG)5 and ATG7 post-TAC. Comparable to in vivo results, cardiac myocytes treated with the CD47-activating peptide, 7N3 (10 μmol/L), showed accumulation of LC3 that was blocked by treatment with a CD47 antagonist Ab (clone OX101, 1 μg/mL) (Figure 7F) and a gene-suppressing HDCA3 morpholino (10 μmol/L) (Figure 7H), but not by

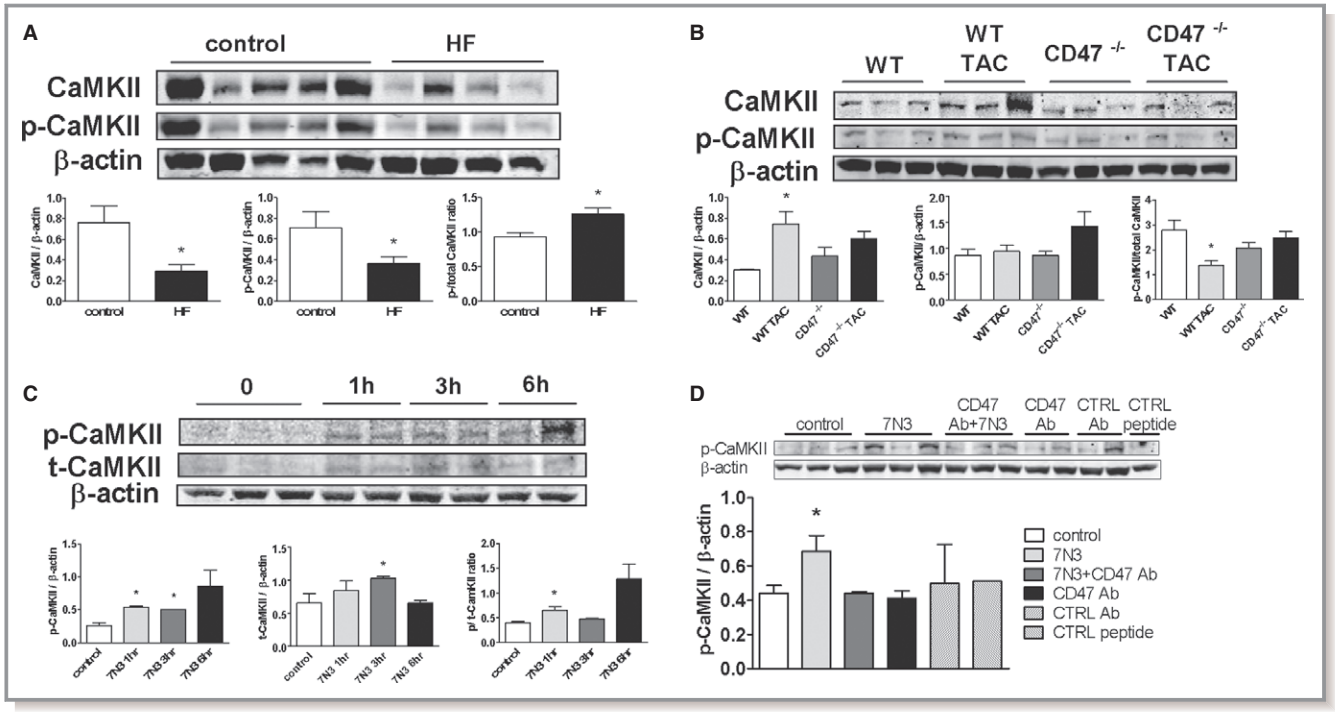

Figure 6. Activated CD47 increases CaMKII expression to increase HDAC3. A, Western immunoblot analysis of CaMKII and phosphorylated CaMKII (p-CaMKII) protein expression in LV tissue samples from patients with nonischemic end-stage LVHF (n=4) and normal controls (n=5). Densitometry is presented as the mean (±SEM). *=statistically significant difference (P<0.05), compared to control. B, Western immunoblot analysis of CaMKII and p-CaMKII protein expression in left ventricular tissue samples from wild-type (WT) and CD47-null animals 4 weeks post-TAC or controls. Densitometry is presented as the mean (±SEM) of n=6 to 9 animals/group. *=statistically significant difference (P<0.05), compared to control. C, Rat neonatal cardiac myocytes (RNCMs) were treated with peptide 7N3 (10 μmol/L) for the indicated time points, and Western immunoblot analysis of p-CaMKII and total CaMKII protein expression was performed. Densitometry is presented as the mean (±SEM) of 3 separate experiments. *=statistically significant difference (P<0.05), compared to control. RNCMs were treated with either a CD47 antibody (D; OX101, 1 mg/mL for 48 hours) or the specific CaKMII inhibitor, AIP (E; 10 nmol/L, 30 minutes)±peptide 7N3 (10 μmol/L, 3 hours), and Western immunoblot analysis of p-CaMKII, HDAC3, and phosphorylated HDCA3 (p-HDAC3) was performed. Densitometry is presented as the mean (±SEM) of 3 separate experiments. *=statistically significant difference (P<0.05), compared to 7N3+CD47 Ab treated and 7N3+AIP. F, RNCMs were loaded with the calcium indicator, Fluo-4 AM, treated with peptide 7N3 (10 μmol/L)±tetracaine (0.5 mmol/L) for the indicated time points, and images were acquired. Fluorescent intensity was determined and results are expressed as the mean±(SEM) from the analysis of cells within a minimum of 7 to 11 regions of interest per culture dish per treatment group. Significant difference (P<0.05) between treatment groups 7N3, compared to 7N3+tetracaine, from 17 through 30 minutes. G, Western immunoblot analysis of total and phosphorylated PLB (p-PLB) protein expression in left ventricular tissue samples from WT and CD47-null animals 4 weeks post-TAC or controls. Densitometry is presented as the mean (±SEM) of n=4 to 6 animals/group. *=statistically significant difference (P<0.05), compared to control; #=statistically significant difference (P<0.05), compared to WT TAC. AIP indicates autocamtide-2-related inhibitory peptide; CaMKII, calcium/calmodulin-dependent protein kinase II; LVHF, left ventricular heart failure; TAC, transverse aortic constriction.

the CaKMII inhibitor, AIP (10 nmol/L) (Figure 7G). Inhibiting Ca^{2+} channels of myocytes with amiloride, but not nifedipine, limited the 7N3-stimulated increase in LC3 (Figure S6A and S6B).

CD47 Blockade Results in Decreased HDAC3 Expression and Corrects Established LVHF

Results in CD47-null animals show the priority of activated CD47, through HDAC3, in promoting LVHF. However, they do not provide insight into CD47 as a therapeutic target for LVHF treatment. We challenged WT ($CD47^{+/+}$) mice with TAC, confirmed established LVHF 1 week later, and then treated animals with a CD47 antagonist Ab (clone 301, 0.4 μg/g body weight IP weekly for 4 weeks).[34] Animals receiving the CD47 Ab displayed mitigation of cardiac myocyte hypertrophy (Figure 8A), decreased LV fibrosis (Figure 8B), and no increase in LV weight post-TAC (Figure 8C). Similarly, treatment with a CD47 antagonist Ab significantly decreased ventricular stiffness (dP/dt min) (Figure 8C), normalized TAC-mediated changes in the pressure volume loop profile (Figure 8D), and attenuated HF-associated LV increases in HDAC3 and CaMKII protein expression (Figure 8E and 8F). In cell cultures, treatment

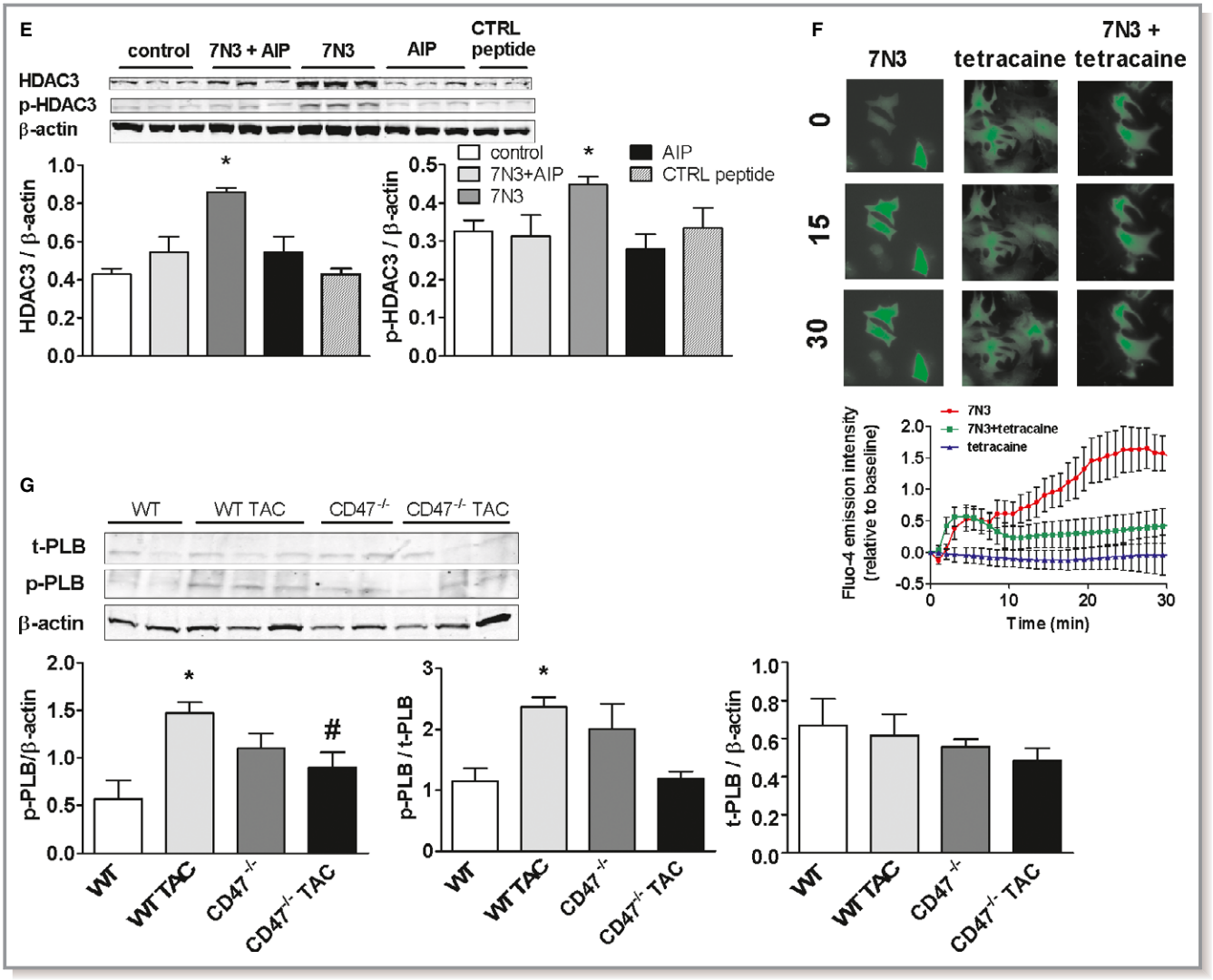

Figure 6. (Continued).

with a CD47 antagonist Ab mitigated 7N3-stimulated cardiac myocyte hypertrophy (Figure 8G). Analysis of LV tissue sections from post-TAC animals treated with a CD47 antagonist Ab demonstrated decreased TUNEL-positive staining cells, compared to LV samples from untreated post-TAC mice (Figure 8H). Finally, LV tissue samples from post-TAC WT mice treated with a CD47 antagonist Ab demonstrated decreased mRNA levels of the downstream target genes, ANP and α-SKA, compared to samples from untreated post-TAC animals (Figure S4B and S4C).

CD47 Is Expressed in LV Biopsies From Healthy Subjects and Dysregulated in *End-Stage* LVHF

The role of CD47 in clinical LVHF is unknown. Analysis of biopsies from a cohort of healthy controls demonstrated CD47 expression (Figure S7A), whereas in *end-stage* LVHF, CD47 protein, but not mRNA, was decreased (Figure S7A and S7C). TSP1 mRNA was also decreased in LV samples from patients with *end-stage* disease LVHF, compared to controls (Figure S7B).

Discussion

The results of this study identify the CD47-HDAC3 axis as a promoter of LVHF. In an experimental model of LVHF, the TSP1-CD47-HDAC3-signaling axis was up-regulated in WT animals. In these experiments, animals were routinely flushed with normal saline to remove circulating cells and platelets (as a potential source of TSP1 and CD47) from the vasculature before harvesting of LV tissues. Together, these findings suggest that cardiac myocytes account for the significant up-regulation of the TSP1-CD47 axis in LVHF. Nonetheless, CD47 has been linked to cell migration,[52] and a possible role for interstitial inflammatory cells cannot be completely excluded. In contrast to WT animals, CD47-null mice were resistant to TAC-mediated

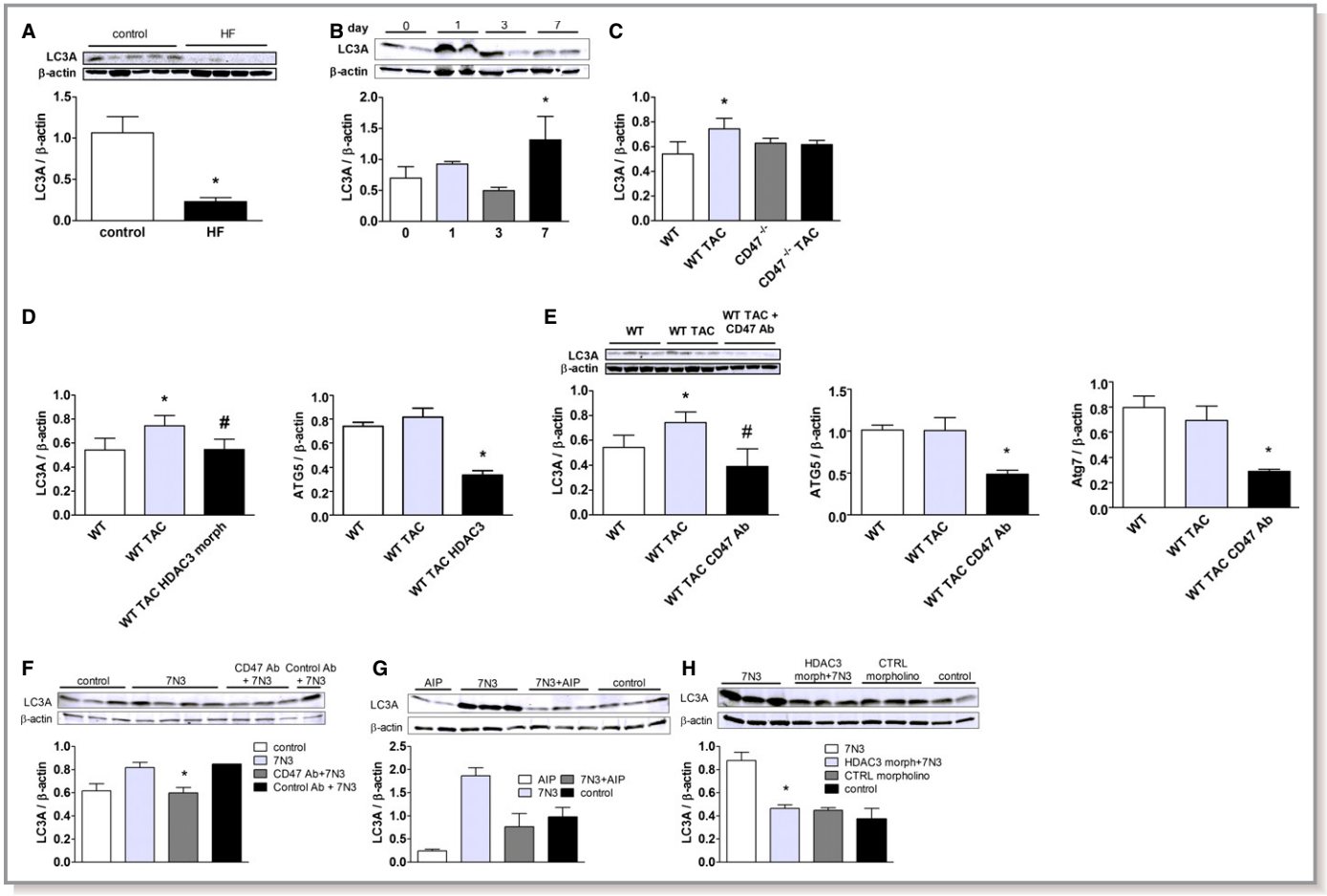

Figure 7. Activated CD47 promotes accumulation of autophagy markers in LVHF. A, Western immunoblot analysis of LC3 protein expression in LV tissue samples from patients with nonischemic end-stage LVHF (n=4) and controls (n=5). Densitometry is presented as the mean of all samples (±SEM). *=statistically significant difference (P<0.05), compared to controls. B, Western immunoblot analysis of LV LC3 protein expression in age-matched male wild-type (WT) C57BL/6 mice pre-TAC and at the indicated days post-TAC (n=3 to 4 animals in each treatment group). Densitometry is presented as the mean (±SEM). *=statistically significant difference (P<0.05), compared to pre-TAC. C, Densitometry of Western immunoblot analysis of LC3 protein expression in LV tissue samples from age-matched male WT and CD47 ($^{-/-}$) null mice 4 weeks post-TAC or control. Densitometry is presented as the mean (±SEM) of n=6 to 9 animals/group. *=statistically significant difference (P<0.05), compared to WT. D, Densitometry of Western immunoblot analysis of LC3, ATG5, and ATG7 protein expression in LV tissue samples from WT mice post-TAC±an HDAC3 morpholino (7 mg/kg body weight) or (E) a CD47 antagonist antibody (Ab; clone 301, 0.4 mg/kg body weight). Densitometry is presented as the mean (±SEM) of n=4 to 9 animals/group. *=statistically significant difference (P<0.05), compared to WT; *, #=statistically significant difference (P<0.05), compared to WT TAC. F, Rat neonatal cardiac myocytes (RNCMs) were treated with a CD47 antagonist (clone OX101, 1 mg/mL) or control Ab, (G) AIP (10 nmol/L, 30 minutes), or (H) an HDAC3 morpholino (10 mmol/L)±peptide 7N3 (10 mmol/L), cell lysates were prepared, and Western immunblots for LC3 performed. Densitometry is presented as the mean (±SEM) of 3 separate experiments. *=statistically significant difference (P<0.05), compared to 7N3+CD47 Ab, 7N3+AIP, and 7N3+HDAC3 morpholino, respectively. AIP indicates autocamtide-2-related inhibitory peptide; ATG, autophagy-related gene; HDAC3, histone deacetylase 3; LC3, light-chain 3; LVHF, left ventricular heart failure; TAC, transverse aortic constriction.

pressure overload LVHF concurrent with down-regulation of HDAC3. Interestingly, preliminary analysis of LV biopsies from a small patient cohort (n=4) with *end-stage* LVHF found that TSP1, CD47, and HDAC3 decreased. Though the reasons for this difference, as compared to results obtained in our experimental murine model and in myocyte cell culture experiments, are not clear, it is possible that significant myocytolysis in an *end-stage* HF contributes to the decreased expression levels of these proteins.[53,54] Future studies in right and left atrial and ventricle samples from early versus late HF patients will clarify the role of TSP1, CD47, and HDAC3 in human disease.

Whereas class I[55] and II[56] HDACs have been implicated in cardiac processes, HDAC3 has not previously been linked to cardiovascular disease or HF. Our studies identify a role for HDAC3 in promoting cardiac remodeling and LVHF. We show that activated CD47 is a proximate regulator of HDAC3-driven cellular hypertrophy and also of ventricular fibrosis. In cell culture experiments, treatment with a CD47-activating peptide increased expression of nuclear HDAC3, whereas in vivo,

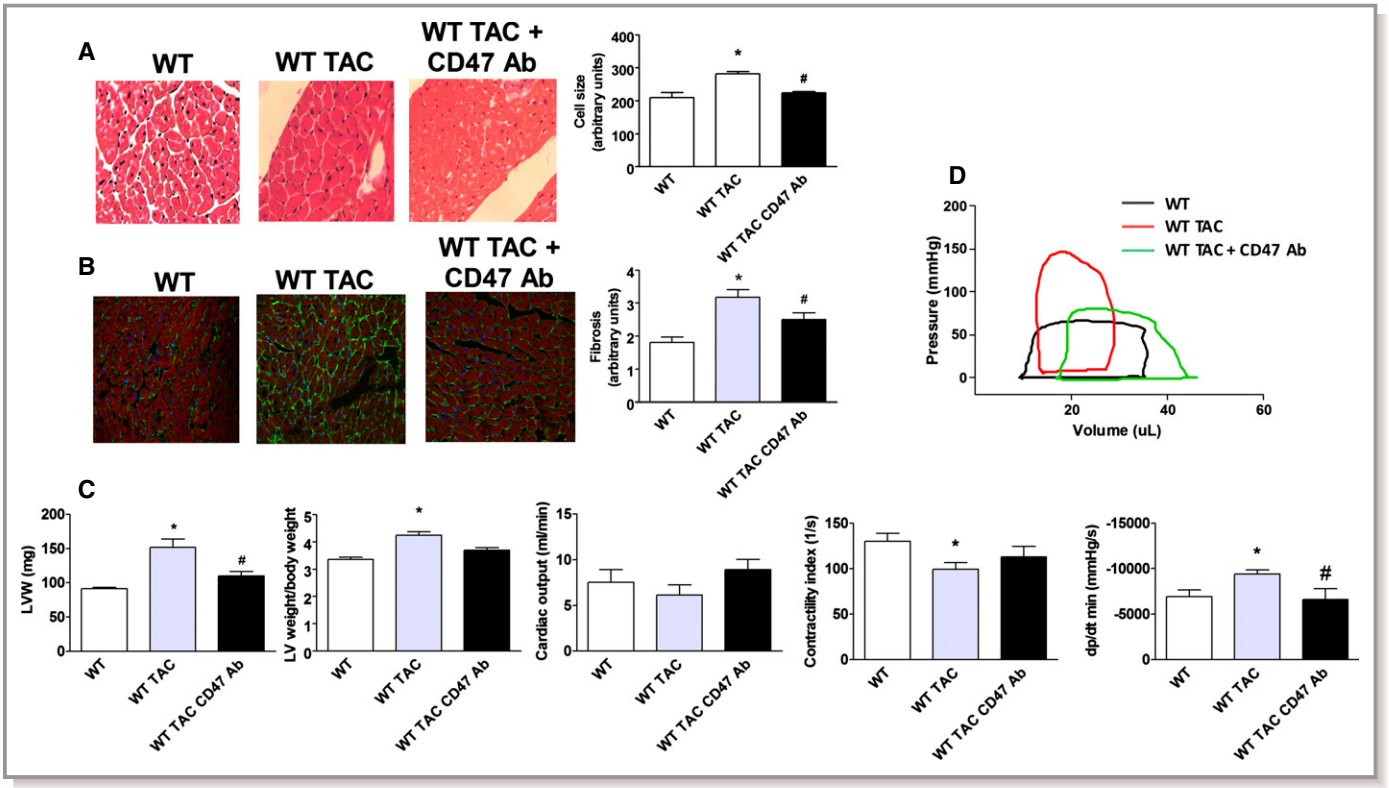

Figure 8. CD47 blockade results in decreased HADC3 expression and corrects established LV HF. (A) H&E staining of murine LV tissue sections from wild-type (WT) mice 4 weeks post-TAC or post-TAC followed 1 week later with a CD47 antagonist antibody (Ab; clone 301, 0.4 μg/g body weight IP) weekly for 3 weeks. Quantification of cell size is presented as the mean (±SEM) of analysis of 4 to 5 slides per animal sample, 10 random hpf per slide, 3 to 4 animals per treatment group. *=statistically significant difference (P<0.05), compared to WT; #=statistically significant difference (P<0.05), compared to WT TAC. Representative images are presented (original magnification, ×40). B, Immunofluorescence staining of murine left ventricle tissue sections 4 weeks post-TAC or control as above indicated in (A). DAPI, collagen I, and phalloidin are colored blue, green, and red, respectively. Fibrosis is calculated as intensity of fluorescence and is presented as the mean (±SEM) of analysis of 3 to 5 slides pre animal sample, 10 random hpf per slide, 4 to 8 animals per treatment group. *=statistically significant difference (P<0.05), compared to WT; #=statistically significant difference (P<0.05), compared to WT TAC. Representative images are presented (original magnification, ×40). C, Left ventricle weight alone and normalized to body weight from animals in treatment groups as indicated in (A). Data are presented as the mean (±SEM) of n=7 to 12 animals/group. *=statistically significant difference (P<0.05), compared to WT; #=statistically significant difference (P<0.05), compared to WT TAC. Assessment by open-chest pressure volume loop analysis of cardiac output, contractility, and ventricular stiffness (dp/dt min) of animals from indicated treatment groups. Data are presented as the mean (±SEM) of n=7 to 12 animals/group. *=statistically significant difference (P<0.05), compared to WT and WT TAC, respectively; #=statistically significant difference (P<0.05). compared to WT TAC. D, Representative pressure volume tracings from WT, WT TAC, and WT TAC+CD47 Ab-treated mice. Western immunoblot analysis of HDAC3 (E) and CaMKII (F) protein expression in LV samples from animals in the indicated groups. Densitometry is presented as the mean (±SEM) of n=4 to 5 animals/group. *=statistically significant difference (P<0.05), compared to WT; #=statistically significant difference (P<0.05), compared to WT TAC. G, Rat neonatal cardiac myocytes were treated with CD47 antagonist Ab (clone OX101, 1 mg/mL) or immunoglobulin G (IgG) control antibody±peptide 7N3 (10 μmol/L) for 48 hours, and cell size was determined. Representative images are presented (original magnification, ×40). Data are presented as the mean (±SEM) of 4 separate experiments. *=statistically significant difference (P<0.05), compared to IgG; #=statistically significant difference (P<0.05), compared to IgG+7N3. H, TUNEL staining of murine LV tissue sections from WT and 4 weeks post-TAC animals with and without CD47 antagonist Ab treatment. Data are presented as the mean (±SEM) of the ratio of TUNEL-positive cells over total nuclei from analysis of 4 to 5 slides per animal sample, 10 random hpf per slide, 3 to 4 animals per treatment group. *=statistically significant difference (P<0.05), compared to WT TAC. I, Schematic: Secreted TSP1 binds to cardiac myocyte CD47, stimulating extracellular movement of calcium through L-type channels. This leads to ryanodine receptor (RyR2)-mediated calcium efflux from the sarcoplasmic reticulum, activating CaMKII to up-regulate HDAC3 and promote myocyte hypertrophy and LVHF. CaMKII indicates calcium/calmodulin-dependent protein kinase II; DAPI indicates 4',6-diamidino-2-phenylindole; HDAC3, histone deacetylases; H&E, hematoxylin and eosin; LVHF, left ventricular heart failure; TAC, transverse aortic constriction; TSP1, thrombospondin 1; TUNEL, terminal deoxynucleotidyl transferase dUTP nick end labeling.

nuclear HDAC3 expression was decreased post-TAC in CD47-null LV samples, compared to WT. Similarly, treatment of cardiac myocytes with a CD47 antagonist Ab inhibited PE-stimulated induction of HDAC3. PE is known to promote multiple responses, including cellular hypertrophy and HF, and indicate a possible wider role for CD47 in cardiac processes.

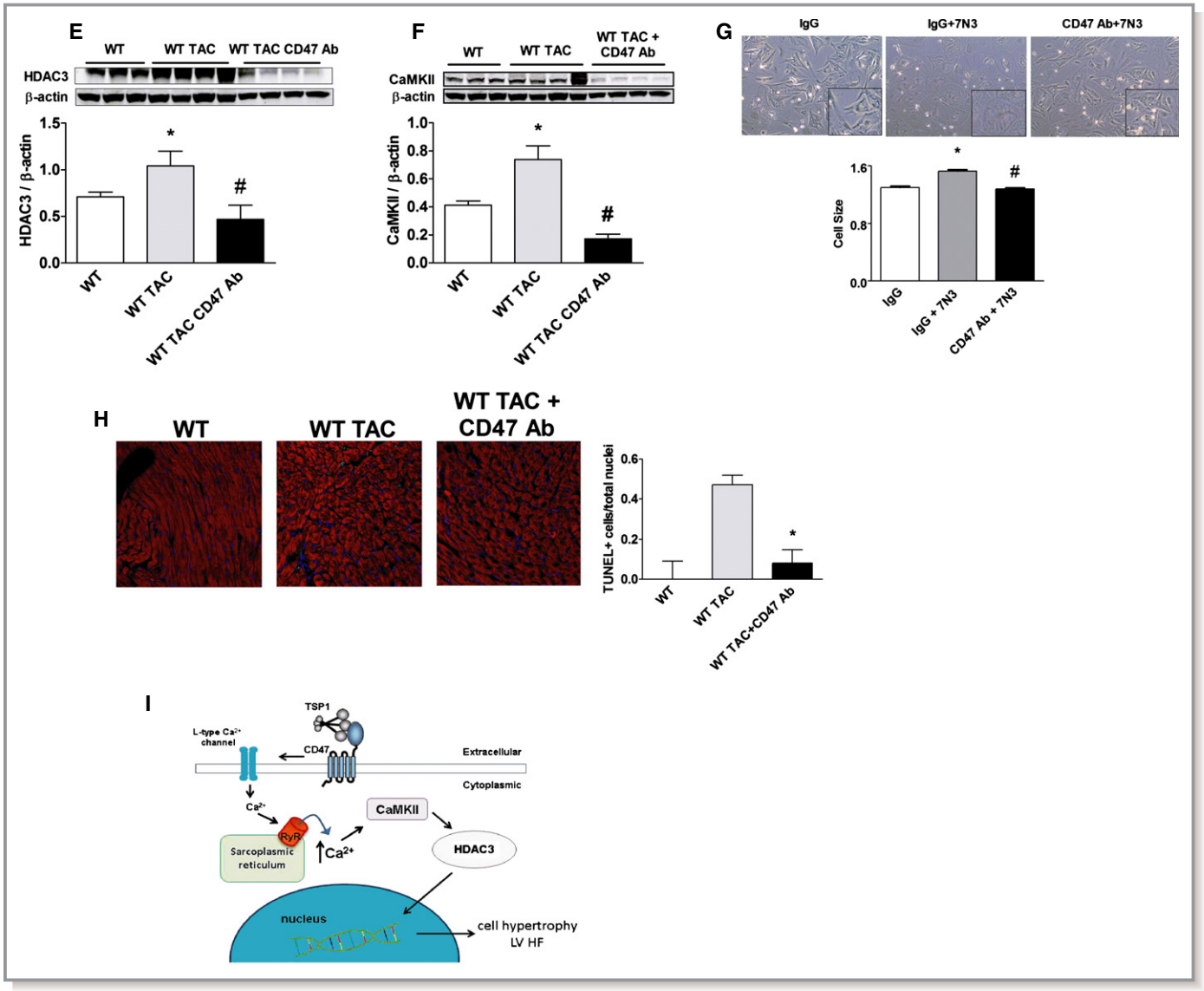

Figure 8. (Continued)

HDAC3 is also known to be sensitive to stimulation by ROS and a proximate activator of tumor necrosis factor alpha in its own right.[57] This is of some importance in light of a recent role we have reported for TSP1, through CD47, as an activator of NADPH-oxidase–mediated ROS production in vascular cells,[13] and suggests multiple nonexclusive mechanisms by which CD47 may up-regulate HDAC3 to promote LVHF.

Activation of CD47 by a TSP1-derived peptide stimulated increased cardiac myocyte CaMKII expression, and this process was abrogated after treatment with a Na^+/Ca^{2+} exchanger and an L-type Ca^{2+} channel blocker. Conversely, specific pharmacologic inhibition of CaMKII activity blocked CD47-mediated up-regulation of HDAC3, identifying HDAC3 as a downstream target of CaMKII. On further investigation, live cell imaging found that activation of myocyte CD47 resulted in a rapid increase in cytoplasmic Ca^{2+}, and that this was, in part, mediated by RyR2 receptors because tetracaine ablated this effect. Together, these new data suggest that cardiac CD47 functions to regulate calcium channel activity and intracellular cytosolic calcium levels in cardiac myocytes (see Figure 8I). Along with results obtained in endothelial cells,[12] these data also suggest that TSP1 and CD47 may regulate Ca^{2+} in multiple cell types in the cardiovascular system.

TSP1 is the prototypic family member of several related TSPs, including TSP2 and -4.[26] The role of matricellular proteins generally, and TSPs specifically, in heart disease remains a focus of ongoing investigation. In a TAC model, TSP1-[58] and TSP4-null mice[59,60] (that, presumably, express cardiac CD47) were reported to develop LV hypertrophy (LVH). These results are interesting in light of our new data and may be explained somewhat by our previous report that TSP1, -2, and -4 all bind to and activate CD47, though with varying affinities.[27] Under TAC-mediated conditions, redundant activation of CD47 by other TSP family members would

be predicted to promote LVH. However, the absence of CD47 (a high-affinity receptor of TSP1, and also a receptor for TSP2 and -4), confers protection from TAC-induced LVHF. Similarly, disrupting CD47 signaling with an antagonist Ab recapitulated the protective null phenotype in WT ($CD47^{+/+}$) animals post-TAC. It remains to be determined whether targeting of TSP1 and -4 in WT mice by antagonist antibodies or gene suppression alters TAC-derived LVHF. Also, as we have reported that CD47 controls basal[12] and ischemic blood flow,[61,62] and ischemia is known to occur in LVHF,[63] it is interesting to hypothesize that TSP1-mediated activation of CD47 may also limit cardiac blood flow under these conditions.

Interestingly, the autophagy marker, LC3, was increased in the ventricles of WT mice post-TAC, compared to WT control ventricles. Conversely, blocking CD47 activation with an Ab or gene suppression of HDAC3 with a morpholino oligonucleotide decreased the TAC-mediated increase in LC3, ATG5, and ATG7 in WT left ventricles. To the best of our knowledge, these data are the first to suggest that HDAC3 contributes, in part, to LVHF through dysregulated autophagy. Recent reports have linked CD47 to radiation-stimulated autophagy[64,65] and, along with our new results, suggest that CD47 may control autophagy under several stress conditions.

Therapeutic intervention of established heart disease is the clinical reality. We found that disrupting the TSP1-CD47-HDAC3 axis at several locations in the signaling cascade decreased myocyte overgrowth, limited ventricular fibrosis, and improved heart function. In the face of established LVHF, a CD47 antagonist Ab, which prevents binding of TSP1 to, and activation of, CD47,[27] suppressed HADC3 expression, improved cardiac function, and lessened LV stiffness. Similarly, gene suppression of HDAC3 reversed established LVHF. These data indicate that both CD47 and HDAC3 are potential therapeutic targets for LVHF. Previous work from our group has identified a role for CD47 in limiting blood flow[7] and metabolism[66] and suggests additional benefits through therapeutic targeting of CD47 in LVHF.

Sources of Funding

This work was supported by NIH grants P01 HL103455, R01 HL-108954, and 1R01HL112914-01A1 and American Heart Association grant 11BGIA7210001 (Isenberg), NIH grants P01 HL103455, U01 HL108642, and 3UL1RR024153 (Champion), and a Ruth L. Kirschstein National Research Service Award (T32 HL098036; Sharifi-Sanjani) and NIH grant UL1-TR-000005. This work was also supported by the Institute for Transfusion Medicine, the Hemophilia Center of Western Pennsylvania, and the Vascular Medicine Institute (Isenberg, Champion). The work was also supported by the NIH grant UL1-TR-000005.

Disclosures

J. S. Isenberg is chair of the Scientific Advisory Boards of Vasculox, Inc (St. Louis, MO) and Radiation Control Technologies, Inc (RCTI; NY, NY) and holds equity interest in the same.

References

1. Stehlik J, Edwards LB, Kucheryavaya AY, Benden C, Christie JD, Dobbels F, Kirk R, Rahmel AO, Hertz MI. The Registry of the International Society for Heart and Lung Transplantation: Twenty-eighth Adult Heart Transplant Report. *J Heart Lung Transplant*. 2011;30:1078–1109.
2. Bueno H, Ross JS, Wang Y, Chen J, Vidan MT, Normand SL, Curtis JP, Drye EE, Lichtman JH, Keenan PS, Kosiborod M, Krumholz HM. Trends in length of stay and short-term outcomes among medicare patients hospitalized for heart failure. *JAMA*. 1993-2006;303:2141–2147
3. Ross JS, Chen J, Lin Z, Bueno H, Curtis JP, Keenan PS, Normand SL, Schreiner G, Spertus JA, Vidan MT, Wang Y, Krumholz HM. Recent national trends in readmission rates after heart failure hospitalization. *Circ Heart Fail*. 2010;3:97–103.
4. Bernheim SM, Grady JN, Lin Z, Wang Y, Savage SV, Bhat KR, Ross JS, Desai MM, Merrill AR, Han LF, Rapp MT, Drye EE, Normand SL, Krumholz HM. National patterns of risk-standardized mortality and readmission for acute myocardial infarction and heart failure. Update on publicly reported outcomes measures based on the 2010 release. *Circ Cardiovasc Qual Outcomes*. 2010;3:459–467.
5. Jugdutt BI. Aging and heart failure: changing demographics and implications for therapy in the elderly. *Heart Fail Rev*. 2010;15:401–405.
6. Hunt SA, Abraham WT, Chin MH, Feldman AM, Francis GS, Ganiats TG, Jessup M, Konstam MA, Mancini DM, Michl K, Oates JA, Rahko PS, Silver MA, Stevenson LW, Yancy CW. 2009 Focused update incorporated into the ACC/AHA 2005 Guidelines for the Diagnosis and Management of Heart Failure in Adults A Report of the American College of Cardiology Foundation/American Heart Association Task Force on Practice Guidelines Developed in Collaboration With the International Society for Heart and Lung Transplantation. *J Am Coll Cardiol*. 2009;53:e1–e90.
7. Isenberg JS, Roberts DD, Frazier WA. CD47: a new target in cardiovascular therapy. *Arterioscler Thromb Vasc Biol*. 2008;28:615–621.
8. Rogers NM, Yao M, Novelli EM, Thomson AW, Roberts DD, Isenberg JS. Activated CD47 regulates multiple vascular and stress responses: implications for acute kidney injury and its management. *Am J Physiol Renal Physiol*. 2012;303:F1117–F1125.
9. Isenberg JS, Frazier WA, Roberts DD. Thrombospondin-1: a physiological regulator of nitric oxide signaling. *Cell Mol Life Sci*. 2008;65:728–742.
10. Isenberg JS, Ridnour LA, Dimitry J, Frazier WA, Wink DA, Roberts DD. CD47 is necessary for inhibition of nitric oxide-stimulated vascular cell responses by thrombospondin-1. *J Biol Chem*. 2006;281:26069–26080.
11. Isenberg JS, Ridnour LA, Perruccio EM, Espey MG, Wink DA, Roberts DD. Thrombospondin-1 inhibits endothelial cell responses to nitric oxide in a cGMP-dependent manner. *Proc Natl Acad Sci USA*. 2005;102:13141–13146.
12. Bauer EM, Qin Y, Miller TW, Bandle RW, Csanyi G, Pagano PJ, Bauer PM, Schnermann J, Roberts DD, Isenberg JS. Thrombospondin-1 supports blood pressure by limiting eNOS activation and endothelial-dependent vasorelaxation. *Cardiovasc Res*. 2010;88:471–481.
13. Csanyi G, Yao M, Rodriguez AI, Ghouleh IA, Sharifi-Sanjani M, Frazziano G, Huang X, Kelley EE, Isenberg JS, Pagano PJ. Thrombospondin-1 regulates blood flow via CD47 receptor-mediated activation of NADPH oxidase 1. *Arterioscler Thromb Vasc Biol*. 2012;32:2966–2973.
14. Nediani C, Raimondi L, Borchi E, Cerbai E. Nitric oxide/reactive oxygen species generation and nitroso/redox imbalance in heart failure: from molecular mechanisms to therapeutic implications. *Antioxid Redox Signal*. 2011;14:289–331.
15. Sorescu D, Griendling KK. Reactive oxygen species, mitochondria, and NAD(P)H oxidases in the development and progression of heart failure. *Congest Heart Fail*. 2002;8:132–140.
16. van Almen GC, Verhesen W, van Leeuwen RE, van de Vrie M, Eurlings C, Schellings MW, Swinnen M, Cleutjens JP, van Zandvoort MA, Heymans S, Schroen B. MicroRNA-18 and microRNA-19 regulate CTGF and TSP1 expression in age-related heart failure. *Aging Cell*. 2011;10:769–779.
17. Batlle M, Perez-Villa F, Lazaro A, Garcia-Pras E, Vallejos I, Sionis A, Castel MA, Roig E. Decreased expression of thrombospondin-1 in failing hearts may favor ventricular remodeling. *Transplant Proc*. 2009;41:2231–2233.

18. Olson EN, Backs J, McKinsey TA. Control of cardiac hypertrophy and heart failure by histone acetylation/deacetylation. *Novartis Found Symp*. 2006;274:3–12; discussion 13–19, 152–155, 272–156.
19. Kao YH, Liou JP, Chung CC, Lien GS, Kuo CC, Chen SA, Chen YJ. Histone deacetylase inhibition improved cardiac functions with direct antifibrotic activity in heart failure. *Int J Cardiol*. 2013;168:4178–4183.
20. Takimoto E, Champion HC, Belardi D, Moslehi J, Mongillo M, Mergia E, Montrose DC, Isoda T, Aufiero K, Zaccolo M, Dostmann WR, Smith CJ, Kass DA. cGMP catabolism by phosphodiesterase 5A regulates cardiac adrenergic stimulation by NOS3-dependent mechanism. *Circ Res*. 2005;96:100–109.
21. Takimoto E, Champion HC, Li M, Belardi D, Ren S, Rodriguez ER, Bedja D, Gabrielson KL, Wang Y, Kass DA. Chronic inhibition of cyclic GMP phosphodiesterase 5A prevents and reverses cardiac hypertrophy. *Nat Med*. 2005;11:214–222.
22. Feuerstein G, Ruffolo RR Jr, Yue TL. Apoptosis and congestive heart failure. *Trends Cardiovasc Med*. 1997;7:249–255.
23. Cardinale JP, Sriramula S, Pariaut R, Guggilam A, Mariappan N, Elks CM, Francis J. HDAC inhibition attenuates inflammatory, hypertrophic, and hypertensive responses in spontaneously hypertensive rats. *Hypertension*. 2010;56:437–444.
24. McKinsey TA. Therapeutic potential for HDAC inhibitors in the heart. *Annu Rev Pharmacol Toxicol*. 2012;52:303–319.
25. McKinsey TA. Isoform-selective HDAC inhibitors: closing in on translational medicine for the heart. *J Mol Cell Cardiol*. 2011;51:491–496.
26. Roberts DD, Miller TW, Rogers NM, Yao M, Isenberg JS. The matricellular protein thrombospondin-1 globally regulates cardiovascular function and responses to stress via CD47. *Matrix Biol*. 2012;31:162–169.
27. Isenberg JS, Annis DS, Pendrak ML, Ptaszynska M, Frazier WA, Mosher DF, Roberts DD. Differential interactions of thrombospondin-1, -2, and -4 with CD47 and effects on cGMP signaling and ischemic injury responses. *J Biol Chem*. 2009;284:1116–1125.
28. Gao AG, Frazier WA. Identification of a receptor candidate for the carboxyl-terminal cell binding domain of thrombospondins. *J Biol Chem*. 1994;269:29650–29657.
29. Maxhimer JB, Shih HB, Isenberg JS, Miller TW, Roberts DD. Thrombospondin-1/CD47 blockade following ischemia-reperfusion injury is tissue protective. *Plast Reconstr Surg*. 2009;124:1880–1889.
30. Kanwar M, Agarwal R, Barnes M, Coons J, Raina A, Sokos G, Murali S, Benza RL. Role of phosphodiesterase-5 inhibitors in heart failure: emerging data and concepts. *Curr Heart Fail Rep*. 2013;10:26–35.
31. Isenberg JS, Martin-Manso G, Maxhimer JB, Roberts DD. Regulation of nitric oxide signalling by thrombospondin 1: implications for anti-angiogenic therapies. *Nat Rev Cancer*. 2009;9:182–194.
32. Methner C, Lukowski R, Grube K, Loga F, Smith RA, Murphy MP, Hofmann F, Krieg T. Protection through postconditioning or a mitochondria-targeted s-nitrosothiol is unaffected by cardiomyocyte-selective ablation of protein kinase g. *Basic Res Cardiol*. 2013;108:337.
33. Bolger TA, Yao TP. Intracellular trafficking of histone deacetylase 4 regulates neuronal cell death. *J Neurosci*. 2005;25:9544–9553.
34. Isenberg JS, Romeo MJ, Abu-Asab M, Tsokos M, Oldenborg A, Pappan L, Wink DA, Frazier WA, Roberts DD. Increasing survival of ischemic tissue by targeting CD47. *Circ Res*. 2007;100:712–720.
35. Colomer JM, Mao L, Rockman HA, Means AR. Pressure overload selectively up-regulates Ca^{2+}/calmodulin-dependent protein kinase II in vivo. *Mol Endocrinol*. 2003;17:183–192.
36. Backs J, Song K, Bezprozvannaya S, Chang S, Olson EN. CaM kinase II selectively signals to histone deacetylase 4 during cardiomyocyte hypertrophy. *J Clin Invest*. 2006;116:1853–1864.
37. Chu CH, Tzang BS, Chen LM, Kuo CH, Cheng YC, Chen LY, Tsai FJ, Tsai CH, Kuo WW, Huang CY. IGF-II/mannose-6-phosphate receptor signaling induced cell hypertrophy and atrial natriuretic peptide/BNP expression via Galphaq interaction and protein kinase C-alpha/CaMKII activation in H9c2 cardiomyoblast cells. *J Endocrinol*. 2008;197:381–390.
38. Kato T, Sano M, Miyoshi S, Sato T, Hakuno D, Ishida H, Kinoshita-Nakazawa H, Fukuda K, Ogawa S. Calmodulin kinases ii and iv and calcineurin are involved in leukemia inhibitory factor-induced cardiac hypertrophy in rats. *Circ Res*. 2000;87:937–945.
39. Hohl M, Wagner M, Reil JC, Muller SA, Tauchnitz M, Zimmer AM, Lehmann LH, Thiel G, Bohm M, Backs J, Maack C. HDAC4 controls histone methylation in response to elevated cardiac load. *J Clin Invest*. 2013;123:1359–1370.
40. Maier LS, Bers DM. Calcium, calmodulin, and calcium-calmodulin kinase II: heartbeat to heartbeat and beyond. *J Mol Cell Cardiol*. 2002;34:919–939.
41. Marx SO, Reiken S, Hisamatsu Y, Jayaraman T, Burkhoff D, Rosemblit N, Marks AR. PKA phosphorylation dissociates FKBP12.6 from the calcium release channel (ryanodine receptor): defective regulation in failing hearts. *Cell*. 2000;101:365–376.
42. Wehrens XH, Lehnart SE, Reiken SR, Marks AR. Ca^{2+}/calmodulin-dependent protein kinase II phosphorylation regulates the cardiac ryanodine receptor. *Circ Res*. 2004;94:e61–e70.
43. Marx SO, Marks AR. Dysfunctional ryanodine receptors in the heart: new insights into complex cardiovascular diseases. *J Mol Cell Cardiol*. 2013;58:225–231.
44. Minamisawa S, Hoshijima M, Chu G, Ward CA, Frank K, Gu Y, Martone ME, Wang Y, Ross J Jr, Kranias EG, Giles WR, Chien KR. Chronic phospholamban-sarcoplasmic reticulum calcium atpase interaction is the critical calcium cycling defect in dilated cardiomyopathy. *Cell*. 1999;99:313–322.
45. del Monte F, Harding SE, Dec GW, Gwathmey JK, Hajjar RJ. Targeting phospholamban by gene transfer in human heart failure. *Circulation*. 2002;105:904–907.
46. Nishida K, Kyoi S, Yamaguchi O, Sadoshima J, Otsu K. The role of autophagy in the heart. *Cell Death Differ*. 2009;16:31–38.
47. Dhesi P, Tehrani F, Fuess J, Schwarz ER. How does the heart (not) die? The role of autophagy in cardiomyocyte homeostasis and cell death. *Heart Fail Rev*. 2010;15:15–21.
48. Smaili SS, Pereira GJ, Costa MM, Rocha KK, Rodrigues L, do Carmo LG, Hirata H, Hsu YT. The role of calcium stores in apoptosis and autophagy. *Curr Mol Med*. 2013;13:252–265
49. Qipshidze N, Tyagi N, Metreveli N, Lominadze D, Tyagi SC. Autophagy mechanism of right ventricular remodeling in murine model of pulmonary artery constriction. *Am J Physiol Heart Circ Physiol*. 2012;302:H688–H696.
50. Givvimani S, Munjal C, Tyagi N, Sen U, Metreveli N, Tyagi SC. Mitochondrial division/mitophagy inhibitor (mdivi) ameliorates pressure overload induced heart failure. *PLoS ONE*. 2012;7:e32388.
51. Kobayashi S, Xu X, Chen K, Liang Q. Suppression of autophagy is protective in high glucose-induced cardiomyocyte injury. *Autophagy*. 2012;8:577–592.
52. Motegi S, Okazawa H, Ohnishi H, Sato R, Kaneko Y, Kobayashi H, Tomizawa K, Ito T, Honma N, Buhring HJ, Ishikawa O, Matozaki T. Role of the CD47-SHPS-1 system in regulation of cell migration. *EMBO J*. 2003;22:2634–2644.
53. Mann DL, Barger PM, Burkhoff D. Myocardial recovery and the failing heart: myth, magic, or molecular target? *J Am Coll Cardiol*. 2012;60:2465–2472.
54. Turillazzi E, Baroldi G, Silver MD, Parolini M, Pomara C, Fineschi V. A systematic study of a myocardial lesion: colliquative myocytolysis. *Int J Cardiol*. 2005;104:152–157.
55. Gallo P, Latronico MV, Grimaldi S, Borgia F, Todaro M, Jones P, Gallinari P, De Francesco R, Ciliberto G, Steinkuhler C, Esposito G, Condorelli G. Inhibition of class I histone deacetylase with an apicidin derivative prevents cardiac hypertrophy and failure. *Cardiovasc Res*. 2008;80:416–424.
56. Nebbioso A, Manzo F, Miceli M, Conte M, Manente L, Baldi A, De Luca A, Rotili D, Valente S, Mai A, Usiello A, Gronemeyer H, Altucci L. Selective class II HDAC inhibitors impair myogenesis by modulating the stability and activity of HDAC-MEF2 complexes. *EMBO Rep*. 2009;10:776–782.
57. Zhu H, Shan L, Schiller PW, Mai A, Peng T. Histone deacetylase-3 activation promotes tumor necrosis factor-alpha (TNF-alpha) expression in cardiomyocytes during lipopolysaccharide stimulation. *J Biol Chem*. 2010;285:9429–9436.
58. Xia Y, Dobaczewski M, Gonzalez-Quesada C, Chen W, Biernacka A, Li N, Lee DW, Frangogiannis NG. Endogenous thrombospondin 1 protects the pressure-overloaded myocardium by modulating fibroblast phenotype and matrix metabolism. *Hypertension*. 2011;58:902–911.
59. Frolova EG, Sopko N, Blech L, Popovic ZB, Li J, Vasanji A, Drumm C, Krukovets I, Jain MK, Penn MS, Plow EF, Stenina OI. Thrombospondin-4 regulates fibrosis and remodeling of the myocardium in response to pressure overload. *FASEB J*. 2012;26:2363–2373.
60. Cingolani OH, Kirk JA, Seo K, Koitabashi N, Lee DI, Ramirez-Correa G, Bedja D, Barth AS, Moens AL, Kass DA. Thrombospondin-4 is required for stretch-mediated contractility augmentation in cardiac muscle. *Circ Res*. 2011;109:1410–1414.
61. Isenberg JS, Hyodo F, Pappan LK, Abu-Asab M, Tsokos M, Krishna MC, Frazier WA, Roberts DD. Blocking thrombospondin-1/CD47 signaling alleviates deleterious effects of aging on tissue responses to ischemia. *Arterioscler Thromb Vasc Biol*. 2007;27:2582–2588.
62. Isenberg JS, Qin Y, Maxhimer JB, Sipes JM, Despres D, Schnermann J, Frazier WA, Roberts DD. Thrombospondin-1 and CD47 regulate blood pressure and cardiac responses to vasoactive stress. *Matrix Biol*. 2009;28:110–119.

63. Li YH, Hsieh CY, Wang DL, Chung HC, Liu SL, Chao TH, Shi GY, Wu HL. Remodeling of carotid arteries is associated with increased expression of thrombomodulin in a mouse transverse aortic constriction model. *Thromb Haemost*. 2007;97:658–664.

64. Soto-Pantoja DR, Miller TW, Pendrak ML, DeGraff WG, Sullivan C, Ridnour LA, Abu-Asab M, Wink DA, Tsokos M, Roberts DD. CD47 deficiency confers cell and tissue radioprotection by activation of autophagy. *Autophagy*. 2012;8:1628–1642.

65. Soto-Pantoja DR, Ridnour LA, Wink DA, Roberts DD. Blockade of CD47 increases survival of mice exposed to lethal total body irradiation. *Sci Rep*. 2013;3:1038.

66. Frazier EP, Isenberg JS, Shiva S, Zhao L, Schlesinger P, Dimitry J, Abu-Asab MS, Tsokos M, Roberts DD, Frazier WA. Age-dependent regulation of skeletal muscle mitochondria by the thrombospondin-1 receptor CD47. *Matrix Biol*. 2011;30:154–161.